Available online at www.sciencedirect.com
SCIENCE DIRECT®

Fusion Engineering and Design 72 (2004) 35–62

Fusion Engineering and Design

www.elsevier.com/locate/fusengdes

# Exploratory studies of flowing liquid metal divertor options for fusion-relevant magnetic fields in the MTOR facility

A.Y. Ying[a,*], M.A. Abdou[a], N. Morley[a], T. Sketchley[a], R. Woolley[b], J. Burris[a], R. Kaita[b], P. Fogarty[c], H. Huang[d], X. Lao[a], M. Narula[a], S. Smolentsev[a], M. Ulrickson[e]

[a] Mechanical and Aerospace Engineering Department, UCLA, 420 Westwood Pza, Los Angeles, CA 90095-1597, USA
[b] Princeton University, Princeton Plasma Physics Laboratory, Princeton, NJ, USA
[c] Oak Ridge National Laboratory, Oak Ridge, TN, USA
[d] Energy and Power Department, Nanjing University of Aeronautics and Astronautics, Nanjing, PR China
[e] Sandia National Laboratory, Albuquerque, NM, USA

Available online 17 September 2004

**Abstract**

This paper reports on experimental findings on liquid metal (LM) free surface flows crossing complex magnetic fields. The experiments involve jet and film flows using GaInSn and are conducted at the UCLA MTOR facility. The goal of this study is to understand the magnetohydrodynamics (MHD) features associated with such a free surface flow in a fusion-relevant magnetic field environment, and determine what LM free surface flow option is most suitable for lithium divertor particle pumping and surface heat removal applications in a near-term experimental plasma device, such as NSTX. Experimental findings indicate that a steady transverse magnetic field, even with gradients typical of NSTX outer divertor conditions, stabilizes a LM jet flow—reducing turbulent disturbances and delaying jet breakup. Important insights into the MHD behavior of liquid metal films under NSTX-like environments are also presented. It is possible to establish an uphill liquid metal film flow on a conducting substrate, although the MHD drag experienced by the flow could be strong and cause the flow to pile-up under simulated NSTX magnetic field conditions. The magnetic field changes the turbulent film flow so that wave structures range from 2D column-type surface disturbances at regions of high magnetic field, to ordinary hydrodynamic turbulence wave structures at regions of low field strength at the outboard. Plans for future work are also presented.


*Keywords:* Liquid metal; Free surface; Magnetohydrodynamics; Fusion; Divertor

## 1. Introduction

A liquid metal (LM) divertor/first wall may have a number of advantages for near-term experimental plasma devices, particularly if such plasma devices in-

* Corresponding author. Tel.: +1 310 206 8815; fax: +1 310 825 2599.
*E-mail address:* ying@fusion.ucla.edu (A.Y. Ying).

0920-3796/$ – see front matter 
doi:10.1016/j.fusengdes.2004.07.004

**Nomenclature**

| | |
|---|---|
| $B$ | magnetic field vector (T) |
| $d$ | jet (nozzle) diameter |
| $F$ | force |
| $j$ | current density (vector) |
| $L$ | characteristic length |
| $N$ | interaction parameter ($\sigma B^2 L/\rho u$) |
| $P$ | pressure ($N/m_2$) |
| $q$ | scalar variable |
| $Re$ | Reynolds number ($\rho ud/u$) |
| $Re_m$ | magnetic Reynolds number ($\mu_0 \sigma UL$) |
| $t$ | time (s) |
| $\Delta t$ | time step (s) |
| $V,u$ | velocity vector |
| $We$ | Weber number |

*Greek letters*

| | |
|---|---|
| $\delta$ | film thickness |
| $\gamma$ | surface tension |
| $\mu$ | dynamic viscosity |
| $\mu_0$ | magnetic permeability |
| $\rho$ | density |
| $\sigma$ | electric conductivity |

*Subscripts*

| | |
|---|---|
| e | effective |
| g | gravity |
| m | magnetic field |
| o | initial |
| s | surface or interface |
| v | void (wall) |
| T | toroidal |
| $\perp$ | surface normal; vertical |

tend to run long-pulse and high-power discharges. Such conditions would probably result in melting and evaporation of the inertially cooled solid plates, in which subsequent solidification could result in shapes even more prone to overheating. However, at high-enough velocities, liquid metal free surface flows can withstand high heat fluxes with an insignificant amount of evaporation. Furthermore, a liquid lithium wall would be able to pump any incident hydrogen ions or neutrals as well as gettering oxygen and water impurities present in the plasma chamber. This edge pumping action allows density control, and in particular will enable the machine to run in lower recycling regimes, with likely advantages for plasma stability and confinement [1-3]. Nevertheless, a critical question remains: *can free surface liquid metal flow in a desirable fashion across the field of a magnetically confined plasma experiment?*

The issue of establishing viable liquid metal free surface flow configurations in a plasma device relevant magnetic field configuration is the main focus of this study. In particular, the feasibility of such a liquid metal free surface flow is very sensitive to variations in strength and orientation of the magnetic fields. In this paper, we present the initial stage of research conducted under the APEX project to help define a free surface module configuration in an experimental plasma device (e.g. NSTX) [4]. Our approach at defining such a concept couples experimental efforts (specifically in the magnetic torus, LM-MHD [MTOR] facility) with numerical simulations, and focuses on the effects of complex magnetic fields on free liquid metal jets and film flow characteristics. The initial experimental goal is to explore possible flow configurations in steady-state, NSTX-like, spatially varying magnetic fields of the outboard lower divertor region. The module is assumed here to be straight, and positioned as shown in Fig. 1. Note that the initial concept was not to have the entire divertor region covered with lithium, but to con-

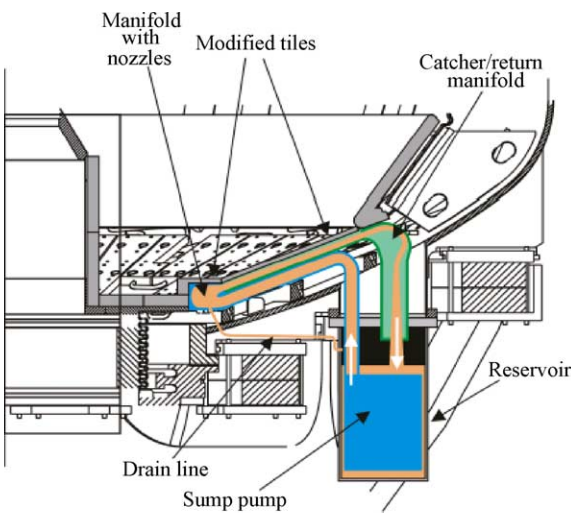


Fig. 1. Proposed lithium free surface module for NSTX outboard divertor.

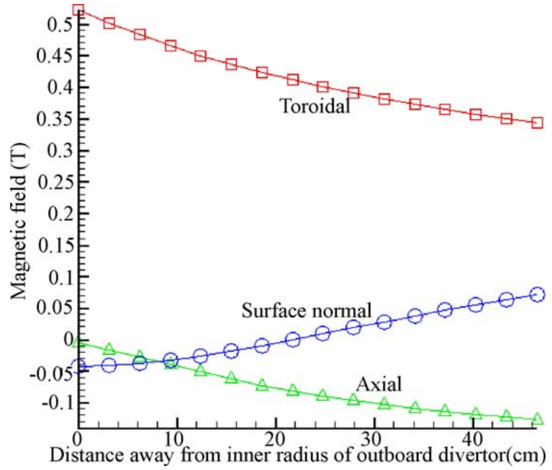


Fig. 2. NSTX magnetic field strengths at outboard divertor region.

sider a module that was limited in its toroidal extent. A variety of different flows comprised of jets and film flows will be explored. In addition, the experiments will provide data for benchmarking computer modeling development efforts [5] on free surface LM MHD flows for both near-term modules and fusion power reactor relevant conditions.

The MHD drag can be significant in a small plasma device, such as NSTX. In particular, the effects caused by gradient fields can be tremendous. Besides non-uniformities (such as the $1/R$ dependence of the toroidal field on the major radius) a noticeable feature of this magnetic configuration is associated with a relatively strong poloidal field varying along the straight flow area. A typical 3D magnetic field profile [6] along the outboard divertor region, which corresponds to plasma discharges of $\beta = 10\%$, is shown in Fig. 2. Quantitatively, the toroidal field strength varies from 0.318 to 0.523 T from the outboard toward the inboard along the divertor plate with the corresponding local normal field component varying from $-0.2$ to 0 T. The magnetic field strength along the fluid direction is relatively small when compared to the other components. Its MHD effect, however, cannot be ignored since the induced current is expected to interact with this field component and create unacceptable flow conditions, such as throwing liquid metal into the plasma chamber core. Based on these field magnitudes, preliminary calculations [7] showed that film flow over the outboard divertor is essentially stopped. Further analysis [8] on film flow over the outboard mid-plane indicated that the interaction between the poloidal return current and the gradient surface normal field can cause the flow to spill over one side of the module while leaving the other side bare. Although the degree of accuracy of such analysis has yet to be determined, it sets the stage for experimental investigations.

In the following subsection, previous results of numerical analysis are first presented in order to lay out the background for the experimental study. This is followed in Section 2 by a description of the MTOR facility and a discussion of scaling analysis of the experimental operating parameters for simulating lithium free surface flows in an NSTX magnetic field environment. Under the present scope of experimental study, both free LM jets and film options are conducted. These results are discussed in Sections 3 and 4. Finally, a discussion on the staged implementation of the use of MTOR for completing the assessment of NSTX lithium free surface flow concept evaluation is presented. Overall, the research goal is to present enough data, through experimental investigations coupled with numerical simulations, to allow the project to proceed with sound conceptual and engineering designs suitable for divertor particle pumping and surface heat removal applications in a near-term experimental plasma device, such as NSTX.

### *1.1. Pre-analysis—some initial numerical simulation results*

The phenomena that govern free surface LM MHD behavior in a multi-field configuration are very complex. Not only has this subject been studied in insufficient detail, but also the existence of several intertwined physical mechanisms (free surface, surface waves, complex current paths, MHD drag, etc.) makes clarifying behavior challenging. Although numerical tools for analyzing both steady and time-varying magnetic field interactions to predict free surface LM MHD are difficult to develop, this task must be accomplished in order to adequately interpret experimental results and to fully understand how liquid metal MHD flows in a fusion device. Without the use of 3D formulations, numerical solutions cannot capture the essential essence of the problems, and will often provide inaccurate information. Numerical simulation becomes even more complicated in low field cases, such as NSTX, since the fields are not strong enough to completely suppress turbulence. Moreover, the magnetic Reynolds number, $Re_{\mathrm{m}}$, in our application is larger than 0.1, signifying that the magnetic field induced by current flowing may be approaching the strength of the applied fields. In view of this, substantial efforts under APEX are dedicated to the development of a 3D numerical tool for the study of MHD. This effort and its status are summarized in Ref. [5]. The difficulties come from the actual description of physical phenomena and from accurate mathematical descriptions of physical phenomena at boundaries and interfaces, as well as proper handling of the numerical challenges encountered in free surface tracking. The objectives of the MHD model and analysis presented in this paper are to bring forth the importance of the experimental study. It serves as a pre-analysis tool for experimental execution. By evaluating numerical results it is possible to cross-check the experimental data and determine whether there are unforeseen effects. This is especially important, since it is not clear what to expect when a liquid metal free surface flow crosses a gradient magnetic field. Additionally, experiments provide data to cross-check numerical formulations and approaches and help to illuminate our understanding of LM MHD free surface flows. Since the pre-analysis effort is not intended to be exhaustive, the numerical approach reported here attempts to build a MHD module into an existing CFD code (FLOW-3D [9] in this case). This approach takes into account that at any given point in time the velocity field of the main hydrodynamic quantity can be directly interacting with the main electromagnetic field without any interference. The main disadvantage associated with this approach is limited accessibility to modify and improve the existing CFD code structure and associated numerical algorithms, which presumably dominate computational efficiency. The greater CPU time needed for analysis limits the usefulness of this technique.

FLOW-3D is a commercial 3D free-surface hydrodynamic code that uses volume of fluid surface tracking and projection methods to explicitly solve Navier–Stokes equations with standard turbulence models (k-e, mixing length, etc.). The MHD effect is reflected in an additional term of Lorentz force in the momentum equation at each time step. In the proposed approach, the MHD Lorentz force caused by the induced current is derived from Ampere's law by solving the induced magnetic field equations. This leads to the following set of governing equations, which express the conservation of mass and momentum:

$$\rho\frac{\partial\vec{u}}{\partial t} + \rho\nabla\cdot(\vec{u}\times\vec{u}) = -\nabla\vec{p} + \nabla\cdot\mu(\nabla\vec{u} + \nabla^{t}\vec{u}) + \rho\vec{g} + \vec{F}_{\mathrm{s}} + (\vec{j}\times\vec{B}), \qquad (1)$$

$$\nabla\cdot\vec{u} = 0 \qquad (2)$$

and the conservation for the magnetic field expressed as:

$$\frac{\partial\vec{B}}{\partial t} - \nabla\times(\vec{u}\times\vec{B}) + \nabla\times\left(\frac{1}{\sigma\mu_{\mathrm{m}}}\nabla\times\vec{B}\right) = 0, \qquad (3)$$

$$\nabla\cdot\vec{B} = 0 \qquad (4)$$

where the magnetic field $B$ includes both the applied ($B_o$) and induced ($B'$) fields. The induced current can be deduced from the following equation:

$$\vec{j} = \frac{1}{\mu_{\mathrm{m}}}\nabla\times\vec{B} \qquad (5)$$

A detailed description of the mathematical formulation and numerical technique can be found in Refs. [10,11]. Specifically, the technique applies a conservative formula similar to Salah et al. [12], which leads to the introduction of a penalty factor to impose the local divergence-free condition of the magnetic fields. Furthermore, to improve treatment of the boundary conditions on the induced magnetic field, an extended insulating void is applied around the liquid flow in the computational domain. However, because of the complexity involved in defining electrical and magnetic properties at the fluid/free surface, as well as at the fluid/solid interfaces, only insulated boundary conditions are considered. Presently, the technique has been used in steady-state calculations due to the enormous CPU time requirements.

Calculations from FLOW-3D/MHD that have pointed out what experimental results might look like are summarized in this section, although more results can be found in various APEX presentations [http://www.fusion.ucla.edu/apex] and Refs. [10,11].

#### 1.1.1. Case A: Simple field gradient effects on liquid metal jets

One distinct effect resulting from the passage of a liquid metal jet through a transverse field with strong

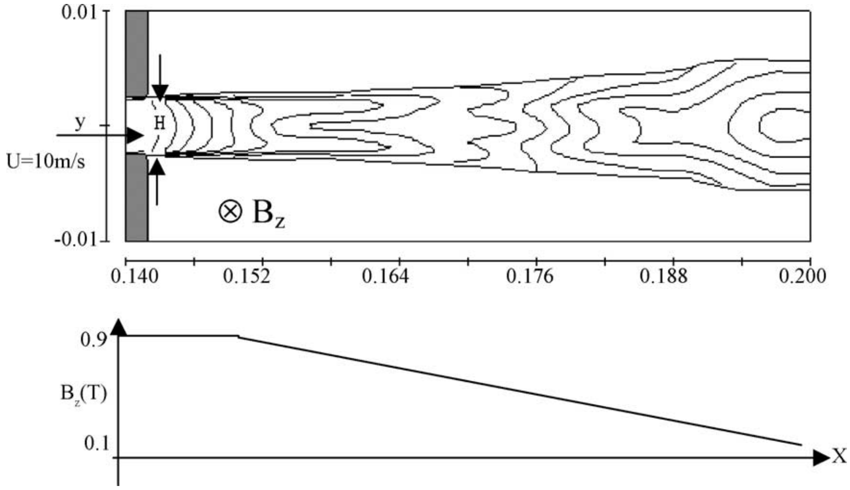


Fig. 3. Calculated GaInSn MHD jet evolution under 1D gradient transverse field. Contour lines are *u* velocity.

gradient in the flow direction is the change in the liquid metal cross-section. In the calculation presented here, a lithium jet flowing out of an insulated nozzle of 5 mm diameter at 10 m/s is set to pass through an external magnetic field which varies along the streamwise direction as shown in Fig. 3. The gradient field magnitude ($\mathrm{d}\vec{B}/\mathrm{d}\vec{x}$) is about 9 T/m, which is stronger than that of NSTX or MTOR field values. As shown, the MHD drag is not sufficient to stop this three-dimensional jet. Rather, its cross-section deforms in such a way that the momentum flux of the jet is conserved. This feature of the jet cross-section deforming is the result of gradient field-induced (*x*-direction) return current interacting with the field itself to produce a transverse force, in which quantity cannot be determined when a 2D model is utilized.

The calculated cross-sectional return current profiles at different downstream locations are shown in Fig. 4. These induced currents circulate within the bulk and build two closing current loops symmetrically around the *y*-axis. This closing of the current paths has a profound influence on the development of the jet. First, the recirculating directions of the return current ($J_x$) in any cross-section are reverse, so the interaction between the $J_x$ and applied magnetic field, $B_z$, results in two opposite Lorentz forces symmetric on the *y*-axis, as shown in Fig. 5. This causes the jet cross-section to be enlarged along the *y*-direction. Meanwhile, the B-parallel Lorentz force, $F_z$, is zero. Under these conditions, we find that the cross-section shape of the jet changes continuously to an oval cross-section. Since the net integral effect of the interacting force is zero

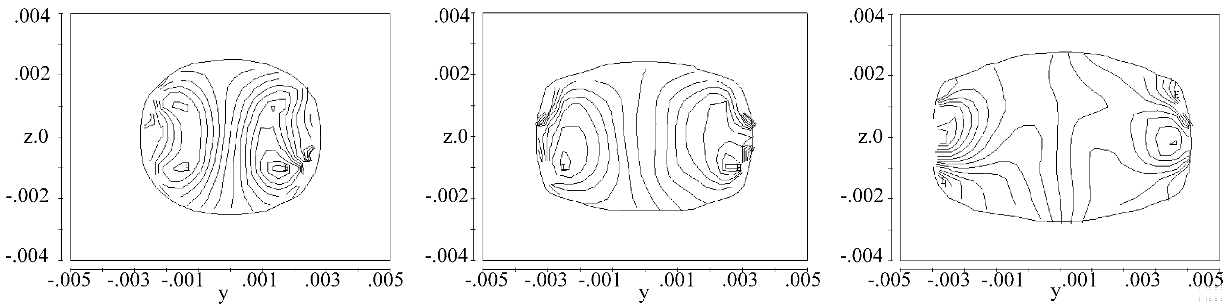


Fig. 4. Induced current $j_x$ contour at *YZ* cross-section of *x* at 0.16, 0.17 and 0.18 m, respectively.

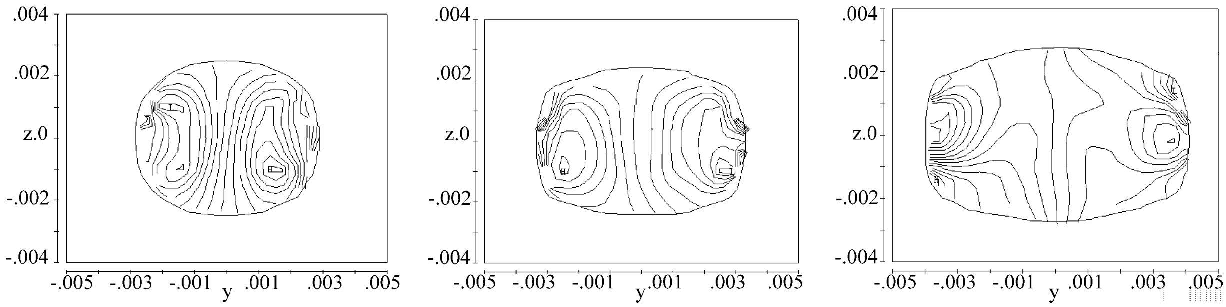


Fig. 5. Contour plots of Lorentz forces $F_y$ at $YZ$ cross-sections of $x$ at 0.16, 0.17 and 0.18 m, respectively.

with respect to each cross-section, this implies that the momentum flux of the jet is conserved, as shown by Davidson [13].

Another feature of the jet flow is the development of an M-shape velocity profile (see Fig. 3), similar to that of closed-channel MHD flow. The formation of the M-shape velocity is a consequence of the interaction between the streamwise $u$ velocity and the applied gradient magnetic field. This generates the induced magnetic field in the streamwise direction ($b'_x$) and consequently generates the induced currents in the transverse direction ($J_y$). The impact on the flow is a Lorentz force opposing fluid flow in the core to cause the fluid to decelerate, while accelerating the fluid flow in the boundary layers.

### 1.1.2. Case B: LM film passing through a 3D magnetic field

As noted, if there is variation of the surface normal field along the streamwise direction, the electrostatic potential as the result of the $\vec{u} \times \vec{B}$ term in Ohm's law will also have a streamwise variation. This leads to a streamwise electric field, which drives current flow in the fluid flow direction. Since the return currents are flowing perpendicular to field lines (surface normal field in this case), the fluid would be propelled by $\vec{j} \times \vec{B}$ forces. Although this tends to create a velocity, $\vec{u} \times \vec{B}$ cancels the electric field, which drives the currents, and thus shuts the currents off and reduces damping. However, to cancel the field, the induced velocities in the normal and spanwise directions must be significantly high, which could potentially cause fluid to be thrown into the plasma core and spill over the side of the module, respectively. These flow perturbations are certainly unacceptable for divertor application, which require that flows stay within the module.

Calculations using FLOW-3D/MHD have been performed to examine this situation. The calculated results of the lithium free surface film along the NSTX outboard divertor proceeding from a uniform inlet of 10 m/s and an initial film thickness of 2 mm are shown in Fig. 6. Only flow characteristics over the first 10 cm downstream have been numerically obtained due to large CPU time requirements. As shown, at about 8 cm downstream, lithium appears to be pushed to one side of the chute, leaving the other side bare. Again, this feature of spilling over one side of the chute is the result of the streamwise return current induced by the gradient surface normal field interacting with the normal field itself, and cannot be displayed with 2D model calculations. In addition, the velocity drops by a factor of 2 to about 5 m/s at 10 cm downstream.

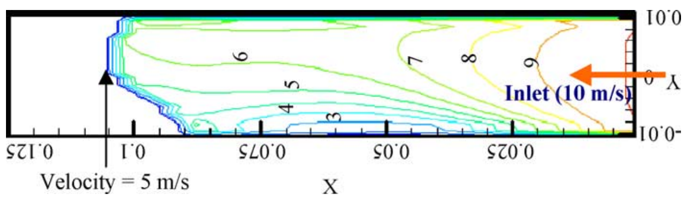


Fig. 6. Calculated lithium MHD ramp flow passing through NSTX outboard divertor fields (2 cm chute with insulated walls). Contour lines are $u$ velocity.

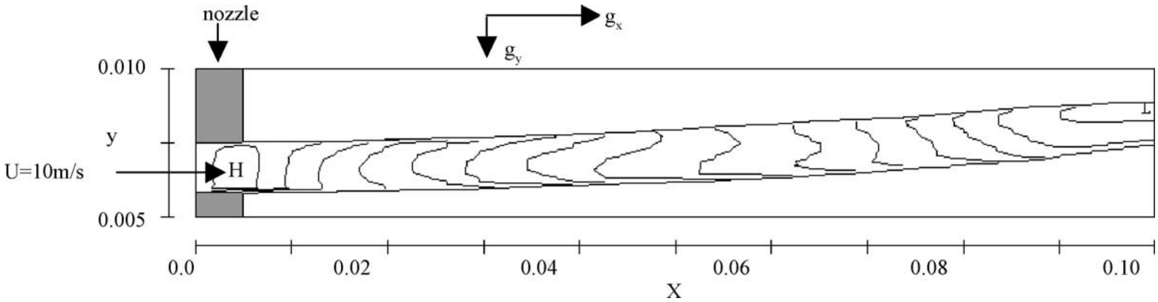


Fig. 7. Calculated lithium jet MHD flow characteristics passing through NSTX outboard divertor fields. Contour lines are *u* velocity.

### *1.1.3. Case C: An LM jet passing through a 3D magnetic field*

A lithium jet ejecting from a nozzle of 5 mm in diameter and passing through the first 10 cm of NSTX outboard divertor fields at a velocity of 10 m/s has been analyzed. It should be noted that all three components of the applied magnetic fields vary along the streamwise direction, as shown in Fig. 2. The calculated MHD jet characteristic is shown in Fig. 7. As shown, the jet has been deflected from its original trajectory along the *y*-axis. This feature is the result of the Lorentz force, $f_y$, being non-symmetric around the *y*-axis and of the fact that the integral of $\vec{j} \times \vec{B}_z$ over the cross-section of the jet being nonzero results in the effects of complex magnetic fields. If indeed the jet would be deflected away from its axis as a consequence of the MHD effect, it would be undesirable for fusion divertor module application.

The accuracy of the calculations and the degree of uncertainty introduced by inadequate treatment of the boundary conditions at the interfaces are not yet known, even with the progress already made in present experimental efforts. Nevertheless, numerical simulation has provided guidance to experimental investigations, such as where to focus. This is particularly useful as far as liquid metal free surface flow experiments are concerned, where diagnostics are extremely limited.

## 2. MTOR facility with flux concentrators and engineering scaling

The MTOR facility was assembled on a limited budget largely from existing equipment, including 24 coils from the TARA device previously at MIT and a dc power supply from PPPL. The 24 TARA coils form a torus, mounted on four-quadrant aluminum-plate stands for access (see Fig. 8). The magnetized toroidal volume has a circular cross-section with major/minor radii $R = 0.78$ m and $a = 0.39$ m. Each TARA coil has two 14-turn windings rated at 3664 A. For initial operation, they are wired in two parallel strings of 12 and each magnet receives approximately 1700 A (which is limited by the available power from the supply). At this current level, the toroidal field strength varies from 0.62 T on the inboard of the torus to 0.21 T on the outboard of the torus. The facility supports initial testing of liquid metal free surface flow concepts without the technical complications and constraints of plasma.

The magnetic system is coupled with a liquid metal flow loop utilizing 15 L of the GaInSn alloy and with an annular induction-type electromagnetic pump that has a maximum flow rate of approximately 3 L/s (which pumps the alloy through the loop). The pump is controlled with a three-phase variable transformer so that flow rate can be controlled as desired. A permanent magnet electromagnetic flow meter was custom built and calibrated using a discharge method to ensure accurate measurements of the bulk flow rate of the system. A custom-built two-tube heat exchanger is utilized to remove excess pump heat from the LM and control the temperature of the working alloy. Thermocouples are attached at several locations to accurately record the LM temperature. A cover gas/vacuum system allows control of the atmosphere in the loop and attached test articles so that the GaInSn sees an inert environment to reduce oxidation and contamination of the alloy and allow experiments at different background atmosphere

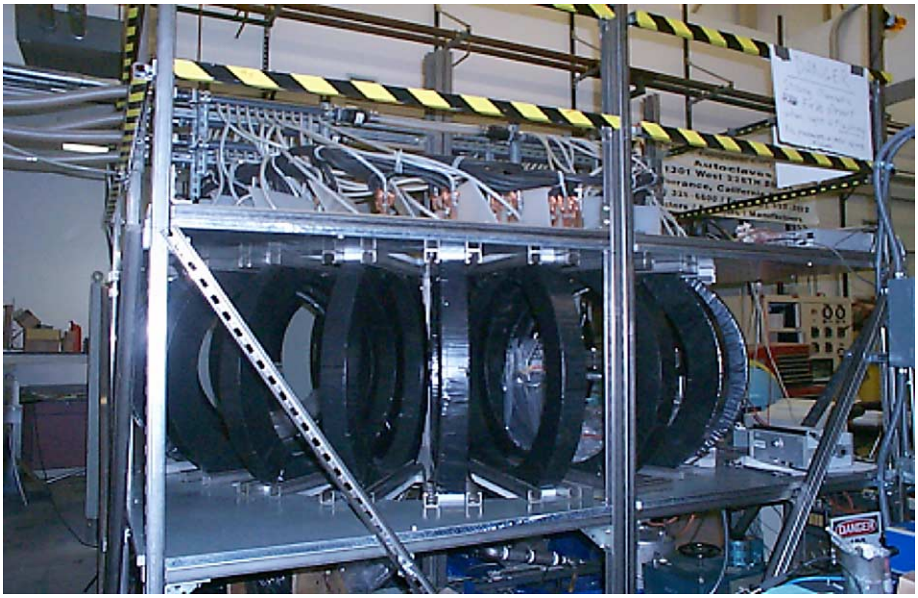


Fig. 8. MTOR Facility constructed with 24 Tara coils.

pressures. A more detailed description of MTOR can be found in Refs. [14,15].

## 2.1. Experiment scaling

MTOR was designed to offer the possibility of very large, even axis-symmetric flow, experiments which are ideal for studying the entire divertor covered by the free surface flow. However, the approach for NSTX was to proceed with a module that was limited in toroidal extent before committing to the whole divertor. This strategy calls for MTOR to be consistent with the NSTX liquid surface module (LSM) time line and adopts a staged approach for executing the MTOR experimental program. In addition, to reduce the safety burden from chemical reactivity of lithium in MTOR, GaInSn is used as the working medium in the initial exploratory stage. This decision to use GaInSn to simulate lithium distorts some of the key MHD lithium flow parameters. Consequently, it is necessary to perform similarity analysis to define prototypical experimental conditions. One apparent difference is that GaInSn is much heavier with higher absolute (dynamic) viscosity (see Table 1). This makes simulation of lithium flow conditions in NSTX more challenging and demands stronger field strengths than NSTX fields.

The key dimensionless parameters that affect MHD free flow characteristics include the Hartmann number *Ha*, interaction number *N*, Reynolds number *Re*, Weber number *We*, and Froude number *Fr*, which are determined by fluid physical properties as well as by operating parameters. The corresponding dimensionless operating parameters for the proposed NSTX lithium free surface module are shown in Table 2. The effects of each dimensionless parameter on fluid flow properties have always been active research topics and have been discussed in the literature. Here, only Weber, Hartmann, and Froude numbers are discussed in order to highlight MTOR experimental operating parameters. The Weber number is the ratio of the inertia force to the capillary force due to the surface tension and is the

Table 1
Properties of lithium and GaInSn

| Property | NSTX | MTOR |
|---|---|---|
| Fluid | Lithium | GaInSn |
| Operating temperature ($T$) (°C) | 225 | 35 |
| Density ($\rho$) (kg/m$^3$) | 485 | 6400 |
| Electrical conductivity ($\sigma$) ($\Omega$m)$^{-1}$ | $2.83 \times 10^6$ | $3.0 \times 10^6$ |
| Surface tension ($\gamma$) (N/m) | 0.325 | 0.533 |
| Absolute viscosity ($\mu$) (kg m/s) | $5.3 \times 10^{-4}$ | $2.05 \times 10^{-3}$ |

Table 2
Jet operating parameters for NSTX and MTOR

| Parameter of interest | NSTX (lithium) | MTOR (GaInSn) | |
|---|---|---|---|
| Field strength (T) | | | |
| Toroidal ($B_T$) | 0.318 to 0.523 | 0.6 to 1.12 (with ion concentrator) | |
| Surface normal ($B_\perp$) | 0.144 to −0.011 | 0.32 to 0 | |
| Axial (longitudinal) | | Not yet simulated | |
| Jet diameter ($d$) (mm) | 5 | 5 | 5 |
| Jet velocity ($V$) (m/s) | 10 | 5 | 3 |
| Flow length ($L$) (cm) | 46 | 45 | 45 |
| Film thickness ($\delta$) (mm) | 2 | 2 | 2 |
| Inclination angle ($\theta$) (°) | 21.5 | 5.5 | 1.85 |
| Hartmann number ($B_T d(\sigma/\mu)^{0.5}$) | 160 | 164 | 164 |
| Reynolds number ($\rho Vd/\mu$) | $4.57 \times 10^4$ | $7.8 \times 10^4$ | $4.6 \times 10^4$ |
| Weber number ($\rho dV^2/\gamma$) | 746 | 1500 | 540 |
| Par. Froude number ($(V^2/g \sin\theta\, L)^{0.5}$) | 7.78 | 7.69 | 7.95 |
| Perp. Froude number ($V^2/g \cos\theta\, \delta$) | 5480 | 1281 | 459 |

characteristic number of the stability of the liquid metal jet.

$$We = \frac{\rho U^2 d}{\gamma} \tag{6}$$

where $\gamma$ is the surface tension. The Weber number is so important that, with it, we can predict the breakup length of the jet with respect to jet flow regime. In a pseudo-laminar jet $\left(\sqrt{We} < 25\right)$, the contraction of surface tension is the disruptive force, and the internal motion is the stabilizing force in that it provides the inertia that delays breakup. On the other hand, in a truly turbulent jet $\left(\sqrt{We} > 25\right)$ where the internal motion is great enough, the surface tension acts as a retarding force (which tends to smooth a roughened surface), while the turbulent motion produces protuberances that tend to disrupt the jet. In the literature, jet breakup length has been correlated with the square root of the Weber number with different empirical coefficients accounting for different jet operating regimes. For example, the square root of the Weber number for a 2 mm diameter, 10 m/s lithium jet being 17 implies that it is a pseudo-laminar jet, in which the breakup is controlled by surface tension capillary instability. According to Phinney's correlation [16], one can expect the jet to break up when it is passing through the 46 cm length of the NSTX outboard divertor region. However, if this lithium jet is 5 mm or greater in diameter, it is not likely be broken before reaching the drain. Thus, if a bank of circular jets is the desired option for the divertor application, each jet should be at least 5 mm in diameter or a higher velocity should be utilized. We will show the modification of this correlation later, while taking into account the MHD effects.

The Hartmann number is the indicator of the magnetic field level strength compared to the viscous force. It is defined as the ratio of the electromagnetic force to the viscous force:

$$Ha = B_0 d \sqrt{\frac{\sigma}{\rho \upsilon}} \tag{7}$$

Here, $B_0$ is the characteristic magnetic field induction and $\sigma$ is the electrical conductivity of the fluid. We can see that the Hartmann number is proportional to the square root of $\sigma/\mu$, and that this value of lithium is twice as high as for gallium. To achieve the same Hartmann number as in NSTX we need to increase the magnetic field of MTOR by a factor of 2. The calculated lithium Hartmann number in NSTX is about 160 (using mean $B$ value). This magnitude of the Hartmann number can be obtained by running GaInSn in a mean magnetic field strength of 0.86 T while keeping the length scale unchanged. Certainly, when dealing with gradient magnetic fields, it is necessary to differentiate whether the dominating effect is controlled by the gradient field strength or by the local magnetic field magnitude. This differentiation is not yet clear in the literature, and is considered to be a central part of research in this study.

The parallel Froude Number defined as:

$$Fr = \frac{u}{\sqrt{gL \sin\theta}}, \tag{8}$$

where $\theta$ is the inclination angle, is the indicator of the gravitational acceleration effect. The parallel Froude number, which corresponds to the NSTX operating condition of lithium flowing at 10 m/s over a 45 cm path at an inclination angle of 21.5°, is about 7.8. This can result in ∼15% acceleration or deceleration (if the design calls for the flow to climb up against the gravity) in velocity without MHD effects. Since gallium alloy is much heavier than lithium, to simulate this effect while preserving the Reynolds number (by running GaInSn at 3 m/s), a near-horizontal MTOR experimental film flow setup (or an inclination angle of 1.85°) is required. When applied to wave and surface behavior, the perpendicular Froude number is defined as the ratio of inertial force to gravity force or the square of Eq. (8) with the substitution of film thickness for flow length and $\cos\theta$ for $\sin\theta$. This definition is particularly important for film flow study, since it determines whether the flow is supercritical (>1) or subcritical (<1). The calculated perpendicular Froude number is significantly high both in NSTX and in MTOR, which implies that both flows are operated in the supercritical flow regime. The experimental operating conditions to reproduce these key dimensionless parameters are listed in Table 2. As shown, MTOR provides adequate capability to study NSTX lithium free surface module flow if the field strength can be increased by a factor of 2.

### *2.2. Flux concentrator design*

To achieve NSTX prototypical field simulation, ferromagnetic structures and permanent magnets are used extensively to provide a locally concentrated magnetic field within MTOR. The basic idea is to collect the flux passing through the cross-section of the torus and distribute this flux into the test region according to the desired flux profile. The collection is accomplished through a large disk of a cold-drawn iron plate. The disks are thick enough so that the flux outside of the concentrator region is largely undisturbed and still has the $1/R$ dependence of a standard magnetic torus. The flux is then redistributed through tailoring "reluctance" by establishing a "reluctance" circuit, in which the test region has a much lower magnetic reluctance than that of the adjacent air gap region (see Fig. 9). Explicitly, an iron flux concentrator was designed with replaceable pole faces to allow a range of field configurations. By shaping and spacing the pole faces of the iron flux concentrator, the magnetic field from the MTOR coils is rearranged locally to produce NSTX-relevant fields for MHD studies. The gap distance and pole-face angle are varied along the liquid flow direction in order to control the field strength and direction in the gap region. These iron flux concentrators (which create desired field strength and orientation) installed in the MTOR facility and are shown in Figs. 10 and 11.

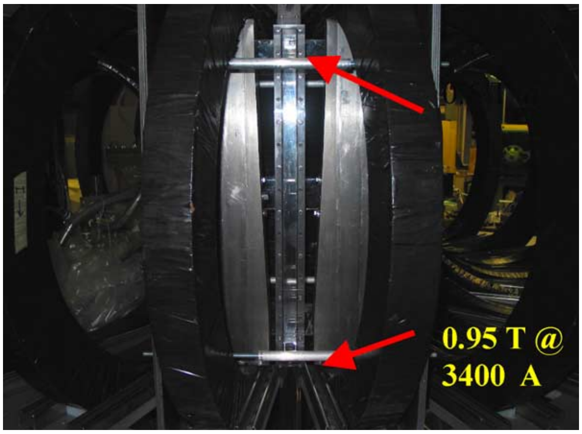


Fig. 9. MTOR experimental set-up with iron flux concentrators for GaInSn jet study (iron flux concentrator with tapered pole faces to create 1D transverse gradient field to simulate gradient toroidal field).

Several sets of pole faces and concentrator sections have been produced and utilized in the experiments described in the following sections. We mention here that it has not proven difficult to effectively double ($B \sim 1.3$ T) the magnetic field magnitude compared to the bare torus so that similarity with NSTX magnetic conditions using the GaInSn alloy are realized. At present, flux concentrator set-ups are placed at two eighth corners of MTOR, as shown in Fig. 12. Here we can clearly see that the space taken for creating a desired magnetic field condition is fairly small (about 1/12). The large test area offered by MTOR allows for the performance of multiple experiments simultaneously.

To further create a 1D gradient field in the test region, the 5-cm-wide iron block pole faces are tapered. This results in distances between the two faces varying from 15 cm at one end to 10 cm on the other end, when they are placed in MTOR as shown in Fig. 9. With this concentrator set-up, the maximum magnetic field at the center of the gap varies from 0.5 to 0.9 T as the gap decreases, whereas the magnetic field gradient is about 0.5 T/m. These ∼5 cm iron blocks are

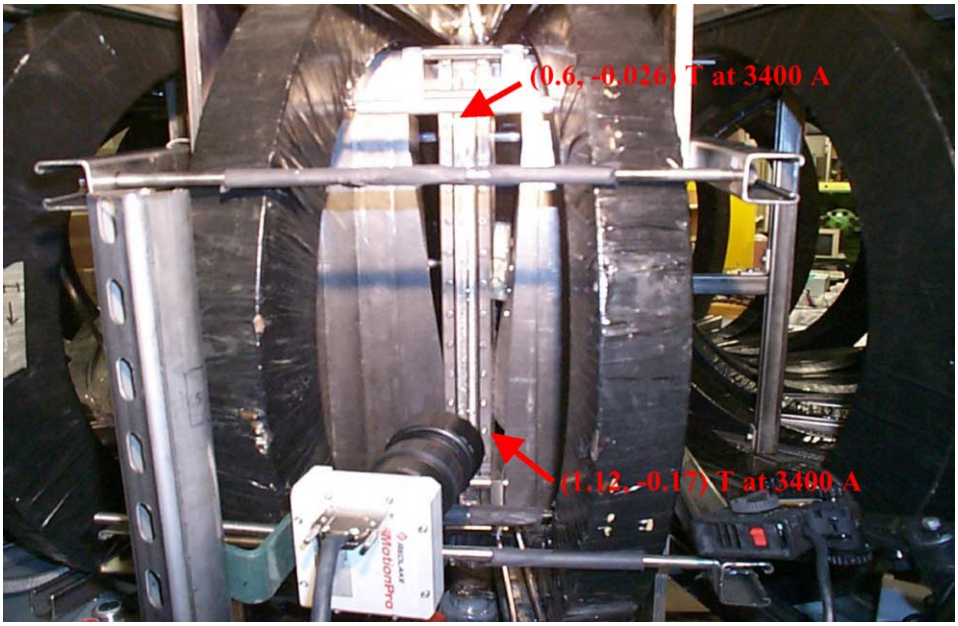


Fig. 10. MTOR experimental setup with iron flux concentrators for GaInSn jet study (iron flux concentrator with twisted-tapered pole faces to create 2D transverse gradient field to simulate gradient toroidal field plus surface normal field).

then shaped with a twisted angle of 21° to provide a 2D field gradient similar to that in NSTX by creating a different gap size not only in the streamwise but also in the spanwise directions. Fig. 11 shows the iron flux concentrators with the twisted-tapered pole face that can simultaneously produce toroidal and surface normal 2D magnetic field gradients. The measured field strength for this set-up gives a toroidal field of 0.6 to 1.12 T with corresponding-radial field values from 0 to 0.17 T. As shown in Fig. 13, these simulated toroidal field strengths appear adequate, although the field strength to simulate the NSTX surface normal component is slightly lower.

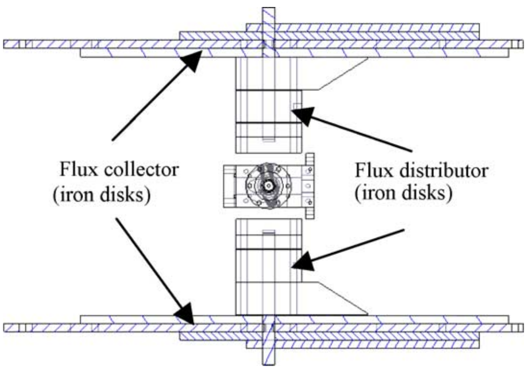


Fig. 11. Top view of iron flux concentrator setup including iron disk for flux collection and iron block pole faces for redistribution of magnetic flux.

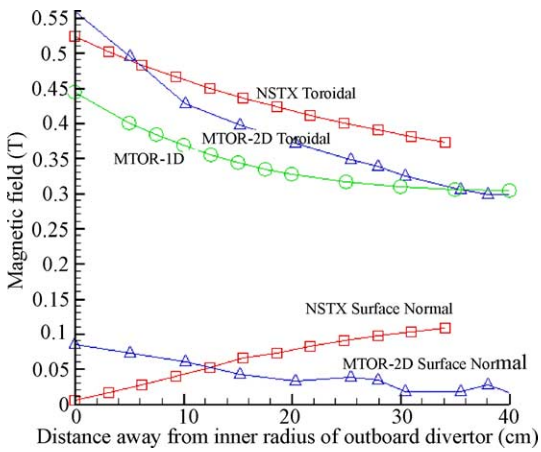


Fig. 12. Scaling corrected MTOR 1D and 2D magnetic field strengths (actual values equal to two times the values shown).

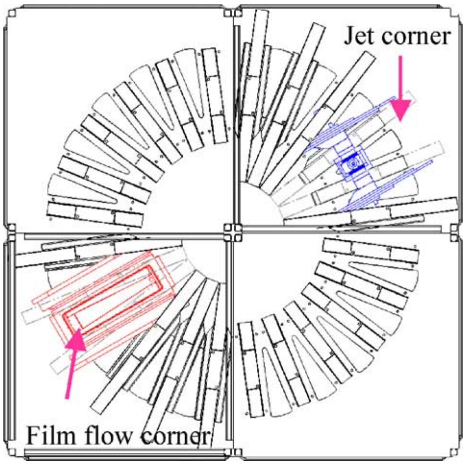


Fig. 13. Top view of MTOR showing two one-sixth fractional core regions of MTOR installed with flux concentrators to enhance field for NSTX simulations.

## 3. Experimental study of liquid metal jets under gradient transverse fields

The use of a bank of circular jets has been considered for fusion divertor application and for the NSTX flowing lithium module. The advantages of using jet configurations over film flow concepts include that there are no drag effects such as Hartmann breaking related to solid walls and that there are no additional cooling requirements for solid edge presence in film divertors with solid walls/dividers. The important issues concerning a flowing liquid metal jet in a complex magnetic field environment relate to the potential for deflection of trajectory, surface instability, cross-section flattening and breakup. These are questions that need to be addressed before putting forward a jet concept for near-term plasma device divertor application.

In recent years, much interest has been taken in the phenomena of liquid metal jets under a magnetic field, due to the potential for application in industry. The experiments performed by Bucenieks et al. [17] showed that in a strong magnetic field free falling jets are essentially stablized; the jet continuity length increases considerably (by 1.5–2 times), and splashing of liquid metal in the receiver is damped. GaInSn has been studied in magnetic fields up to 3.5 T. The jets fell out from non-conducting nozzles with inner diameters of 1–3 mm and lengths of 10–30 mm, while the exit velocity of the jets varied by up to 2 m/s.

Oshima and Yamane [18] studied the shape of a horizontal liquid metal jet under a uniform transverse magnetic field. Tests were performed using both circular and square nozzles. The results showed that changes in the shape of the jet due to surface tension are suppressed under a uniform transverse magnetic field. Ievlev et al. [19] performed an experiment whereby liquid metal jets were laminarized by a coaxial magnetic field. Jet laminarization was accomplished by transition delay, with the joint effect of a coaxial magnetic field and an inlet velocity in the initial cross-section forming a velocity profile with a smooth change at the jet boundary and a low disturbance level. They also showed that at the transition length jet expansion occurs close to the laminar level. At some critical points ($Ha/Re \sim 3.5 \times 10^{-2}$), jet expansion after transition increases suddenly. Subsequently, this growth slackens and the jet becomes stable.

Additionally, Etay et al. [20] performed a study to investigate the mechanism by which the ultimate position of a two-dimensional stream of a liquid metal jet could be controlled. Specifically, the deflection was achieved by the action of the magnetic pressure associated with a high-frequency magnetic field produced by current sources outside the liquid stream. They found that the angle of deflection of the stream could be determined by controlling the power supplied to the perturbing currents. Furthermore, they showed that a current-carrying cylindrical jet could be destabilized by a vertical line current. Extrapolating the results of their study to a lithium liquid metal jet crossing the NSTX magnetic field configuration, it is likely that the jet will be deflected by the MHD forces caused by the longitudinal field component.

In summary, our understanding of how a LM jet performs with respect to MHD effects under various magnetic field orientations and strengths remains limited. LM MHD experiments in a complex field configuration are necessary to help determine the suitability of jets in fusion energy technology applications.

### 3.1. Jet flow experimental setup and test parameters

The major components of the MTOR LM jet study include the test article system, the diagnostics system,

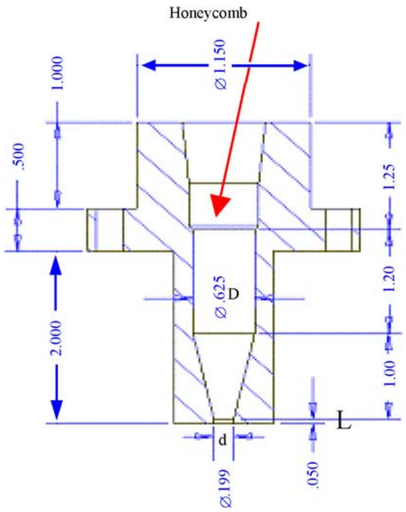


Fig. 14. Nozzle geometry with dimensions.

and the GaInSn flow loop (previously described). The test article system itself includes a short nozzle, which can produce a 5-mm round jet, a transparent test cavity so that the GaInSn jet can be viewed and photographed while still in a controlled atmosphere, and a drain collection, which is designed to minimize liquid build-up and allow liquid to be removed effectively.

Nozzles play a key role in any free jet experiment because they determine initial jet quality and turbulence levels, which in turn dominate surface smoothness and breakup behavior. Assuming constant fluid properties and velocity the main geometrical factors influencing the total velocity distribution at the nozzle exit are (i) the contraction ratio $d/D$, (ii) the nozzle aspect ratio, $L/d$, and (iii) the contraction angle or internal nozzle shape (see Fig. 14 for notation). The flow from the nozzle will always reflect, to a degree, the state of turbulence in the upstream supply. Hence, for any fixed discharge velocity, a decrease in the contraction ratio reduces the general level of turbulence in the core region of the jet. The values of the contraction ratio used in practical situations depend on the circumstances. Sufficiently large values of the contraction ratio would cause higher levels of turbulence in the hose or monitor, resulting in a proportionate level of turbulence to be present in the jet "core flow" [21]. In our experiments, a two-step contraction rate nozzle is used. The first-step contraction ratio is 0.71, and the second-step contraction ratio is 0.32. By using this two-step contraction nozzle, the level of turbulence in the core region of the jet can be greatly reduced.

The presence of a cylindrical section (with length $L$) after the contraction results in the development of shear stress from the no-slip boundary of the solid surface with the fluid. The fluid particles closest to the solid surface are proportionately retarded because of the fluid drag on the nozzle walls, i.e. the flow profile at the end of the contraction is changed to a non-uniform profile at the point of jet formation. If $L/d$ is sufficiently large, then the boundary layer "thickness" eventually reaches a value of $d/2$, i.e. the boundary layer fills the entire tube, resulting in fully developed turbulent pipe flow. Regardless of whether the flow in the cylindrical section of the schematic nozzle is laminar or turbulent, the presence of the cylindrical section is seen to have a profound influence on the velocity profile at the point of jet formation. It would be possible, for instance, for the flow at the end of the contraction to be perfectly smooth; yet the emergent jet may possess a fully developed turbulent velocity profile [21]. To eliminate the boundary layer effect on the core flow, a short section giving an aspect ratio near the nozzle outlet of 0.25 is applied.

Furthermore, in order to prevent the occurrence of boundary layer separation and associate formation of secondary eddies, a contraction angle of about 103° is considered, while all the sharp angles of the nozzle interior are smoothed out. Based on the aforementioned geometrical factors and other effects influencing the total velocity distribution, we designed a three-step short nozzle with a specific contracting section that allows breakup to occur further downstream, as shown in Fig. 14. A honeycomb flow straightener is used to straighten the flow and reduce the initial disturbance. Because the honeycomb structures are arrays of tubular elements arranged parallel to each other and the axis of the free jet, they eliminate and filter out both large-scale transverse velocity components and smaller scale irregularities present in the incoming flow.

The test cavity is made of thick acrylic plate that can handle up to full vacuum and still allow visualization and imaging of the jet during a discharge. The setup equips with a high-speed digital imaging system with a CMOS camera with 1280 pixel × 1024 pixel resolution that provides as high as 1000 frames per second (fps) full resolution, and 10,000 ftp partial resolution. This camera, together with various lenses and light-

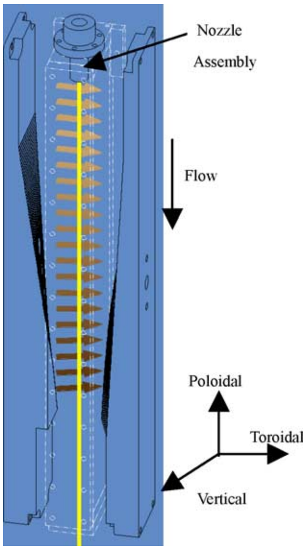


Fig. 15. Schematic view of MTOR jet experimental set-up and orientation description.

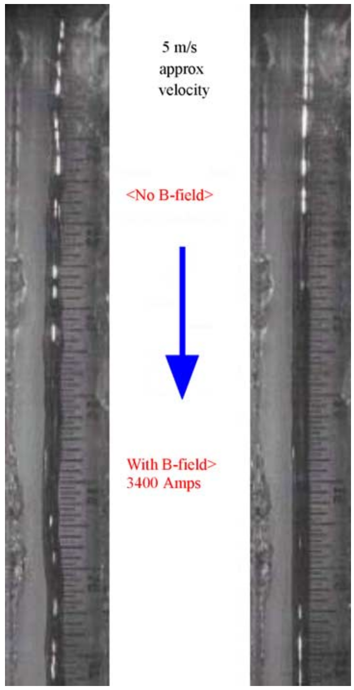


Fig. 16. Poloidal–toroidal view images of GaInSn jet flow characteristics with and without magnetic field (1D gradient field; jet initial velocity = 5 m/s).

ing systems, is used to capture jet trajectories, surface waves and cross-section distortion as the jet proceeds downstream.

Overall, experiments are conducted with jet inlet velocities between 2 and 5 m/s while jets are subjected to 1D as well as 2D transverse gradient fields. The jet is issued from a 5 mm diameter circular nozzle located at the top (where the field strength is the lowest), and proceeds poloidally downstream with increasing field strength as it approaches the collecting drain cone-shape nozzle located at the bottom (Fig. 15). The scaling-corrected MTOR 1D and 2D field magnitudes are shown in Fig. 12. It appears that the MTOR gradient toroidal field is adequate for NSTX simulations. However, note that the fabricated 2D twisted and tapered pole faces do not provide adequate NSTX-prototypical radial field strength in this pole face configuration, which is about two times lower here than the desired values.

### 3.2. Jet flow experimental results

An obvious effect of the transverse magnetic field on a LM jet is to suppress its sausage-like instability structures so that the jet appears like a cylindrical rod (as shown in Fig. 16 for a 5 m/s, 5 mm GaInSn jet passing though a 1D gradient transverse field region). The projected toroidal–poloidal plan images of the liquid metal jet at 55–60 cm downstream in a 2D magnetic field show similar stabilization effects as the magnetic field increases (see Fig. 17). The stabilizing effect of the magnetic field is acting via the suppression by the field of the velocity perturbations. This can be disclosed by observing the images of the poloidal–toroidal plan of the jet shown in Fig. 18, where the light on the image reflects the structures of the vortex existing in the jet. As shown, without the magnetic field, the jet displays a random yet complex vortex structure. These freely turbulent vorticities, are in fact, the source of turbulent jet breakup if the dynamic pressure associated with the jet becomes greater than the pressure due to surface tension. As the current increases, or equivalently the field strength increases, the vortex perpendicular to the field direction is greatly suppressed, leaving the vortex aligned with the streamwise direction. As the characteristic length of the vortex structure becomes smaller with the increase of the magnetic field, the strength of

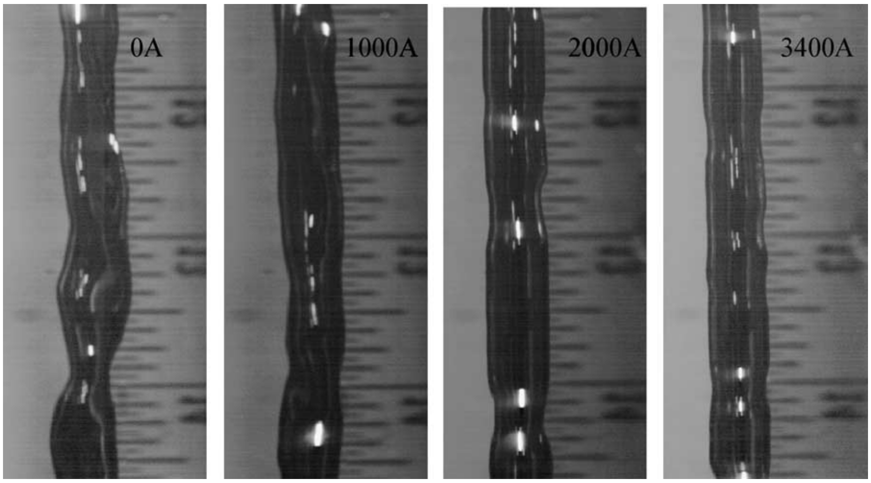


Fig. 17. Poloidal–toroidal view of jet images. GaInSn jet flow characteristics 12–14 in. downstream as magnetic field increases (2D gradient field; jet initial velocity = 3 m/s).

the vortex is also dampened through Joule dissipation. Consequently, this stabilizes the jet.

The motion across magnetic field lines induces a current directed along the vertical axis so that the consequent Lorentz force acts to retard the flow. Figs. 19 and 20 show the width of the jet downstream with and without a magnetic field with an inlet velocity of 3 m/s. Note that here the width of the jet is derived from the jet cross-section at the projected toroidal–poloidal plan image. Thus, it cannot fully represent the cross-section of the jet, since the jet may not be isometric. Nevertheless, we can see that without a magnetic field the width of the jet displays a sinusoidal-like form, which indicates that a great disturbance from surface tension disruptive force exists in the jet. When the magnetic field is on at the maximum MTOR current ($I = 3400$ A), the width of the jet at 8–15 cm downstream becomes a constant, which implies that the mag-

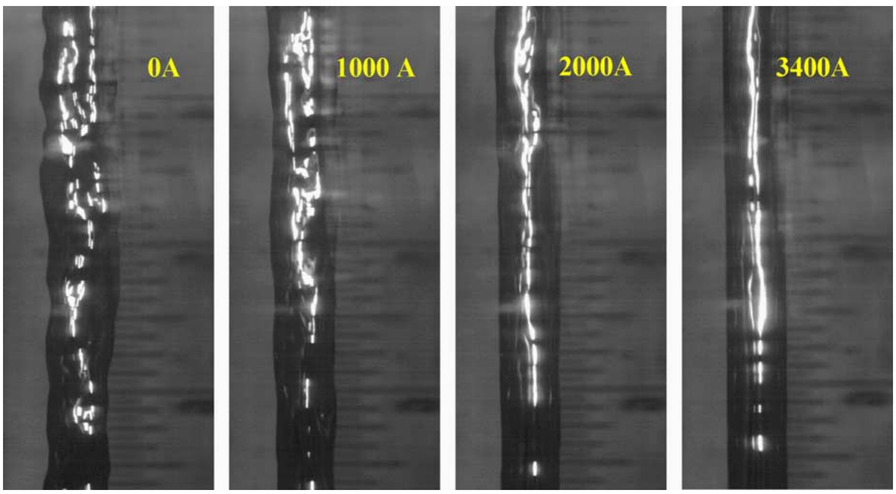


Fig. 18. Poloidal–toroidal view of jet images. Vortex structure evolution as magnetic field increases. (2D gradient field; jet initial velocity = 3 m/s).

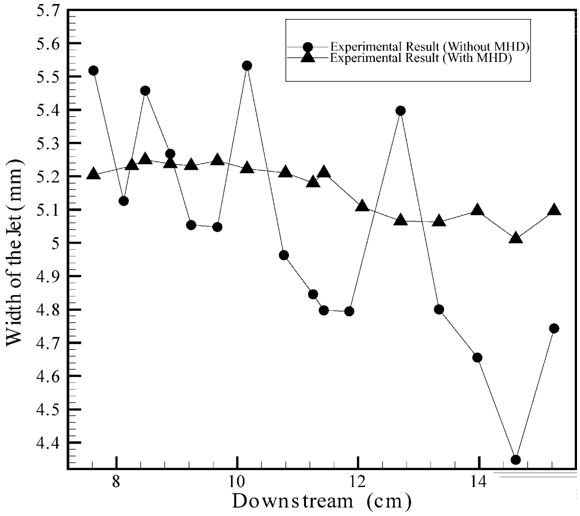


Fig. 19. Jet width evolution 7–15 cm downstream with and without magnetic field (jet initial velocity: 3 m/s).

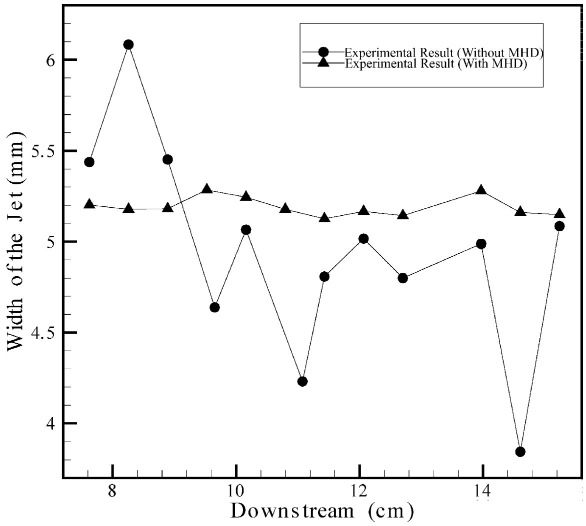


Fig. 21. Jet width evolution 7–15 cm downstream with and without magnetic field (jet initial velocity: 5 m/s).

netic field completely destroys the turbulent motion perpendicular to the field lines. However, at 30–60 cm downstream, the jet displays like sausage indicating that the magnetic constraining force cannot further suppress turbulent momentum, while the surface tension disruptive force overshoots the combined inertial and Lorentz retarding forces. The average width of the jet has increased by about 7% through the Lorentz retarding force even though the gravity wants to accelerate the fluid. Note that the average jet width increase is derived from the jet width comparison between their magnitudes with and without magnetic field at the same downstream location. Unlike the 3 m/s jet where it falls in the pseudo-laminar jet regime, the 5 m/s jet behaves more like a turbulent jet $\left(\sqrt{We} > 25\right)$. Figs. 21 and 22

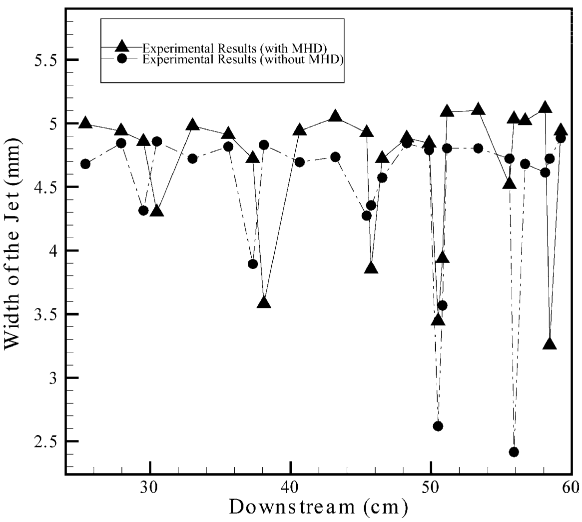


Fig. 20. Jet width evolution 30–60 cm downstream with and without magnetic field (jet initial velocity: 3 m/s).

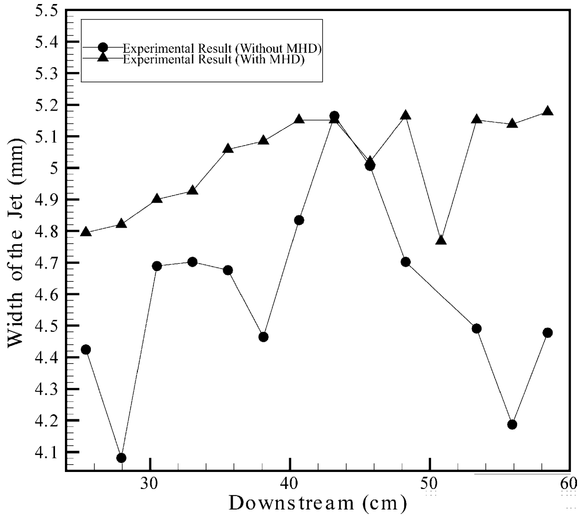


Fig. 22. Jet width evolution 30–60 cm downstream with and without magnetic field (jet initial velocity: 5 m/s).

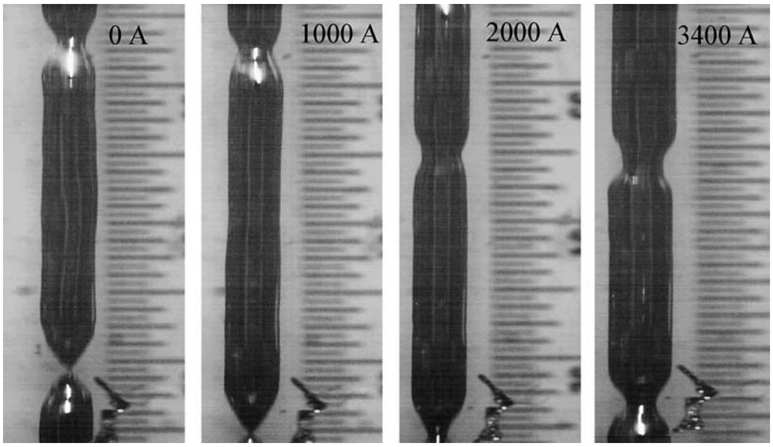


Fig. 23. Jet breakup length increases as magnetic field increases. Poloidal–toroidal view images at 22–24 in. downstream with and without 1D gradient magnetic field (jet initial velocity: 3 m/s).

show the width of the jet downstream with and without a magnetic field. As shown, at 8–15 cm downstream the jet displays a similar shape to that shown in Fig. 19, while the wavelength of the sinusoidal motion is slightly larger. Similar to the 3 m/s case, the oscillation of the width of the jet is significantly reduced by the Lorentz force from the magnetic field. The 5 m/s jet flow at 25–60 cm downstream shows slightly different characteristics than that at 3 m/s. As shown in Fig. 22, there is no evidence of jet breakup in this velocity range because the Weber number of this condition is larger than the previous one, so that the stability length increases accordingly. In addition, the wavelength of the sinusoidal motion is much larger than in Fig. 20. The average width of the jet in this condition increases by 9%, which is slightly larger than the case in 3 m/s. This may be due to the combined effects of inertia and MHD Lorentz force, since both increase with jet velocity.

The stabilizing effect of the magnetic field has resulted in delaying LM jet breakup. This becomes evident by observing the projected toroidal–poloidal plan images of the jet shown in Figs. 23 and 24. These pictures are the front images of a liquid metal jet at 55 to 61 cm downstream in a 1D and 2D magnetic field with

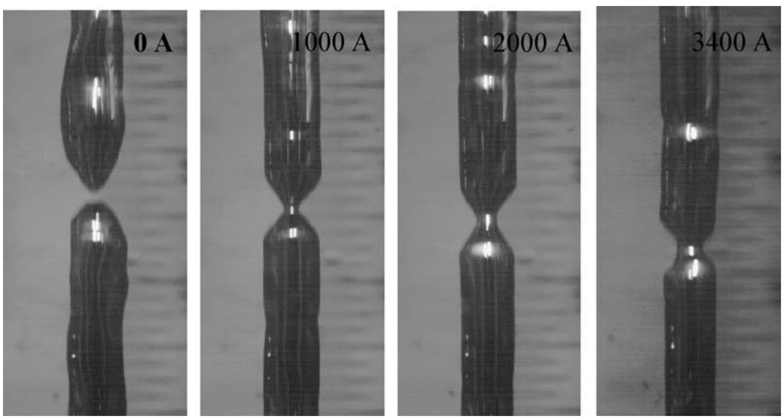


Fig. 24. Jet breakup length increases as magnetic field increases. Poloidal–toroidal view images at 22–24 in. downstream with and without 2D gradient magnetic field (jet initial velocity: 3 m/s).

velocity equal to 3 m/s. The images of the jet shape in the absence of a magnetic field show sinusoidal disturbances due to capillary instability coupled with irregular disturbances having different length scales from the disrupting effects of turbulence. No "break" condition is observed before 55 cm downstream. In addition to a "sausage" shape like jet characteristics, it shows a break up wavelength of about 5–6 jet diameters, which corresponds well to the classic Rayleigh–Weber theory for capillary breakup. With the magnetic field increase, we can see that the "break" point is slightly delayed and the turbulence of the jet is significantly suppressed, accompanied by the absence of secondary modes. The other effect of a magnetic field is a change in the instability growth rate. Unlike with flows in a pure capillary regime, with flows in a magnetic field, the Lorentz force in addition to the inertia force can stabilize the flow. This effect can be seen again in Fig. 23, which demonstrates thickening of the ligaments between two "sausages" as the magnetic field grows. Furthermore, yet to be analyzed, are the limited data showing that the "break" point occurs earlier in a 2D gradient field than it does in a 1D gradient field condition. This implies that the surface normal magnetic field helps break apart the jet. Within the limited data from the MTOR GaInSn runs, breakup was found at inlet velocities lower than 3.2 m/s, in which the jet appears as a pseudo-laminar jet while the square root of the Weber number is less than 25. The observed breakup lengths without and with magnetic field were 57 and 60 cm and 36 and 41.2 cm for initial jet velocity of 3 and 2.1 m/s, respectively. These observations suggest that breakup length with a magnetic field can be expressed as:

$$L = \alpha L_{\text{nofield}}$$

where $\alpha$ is a coefficient related to the Hartmann number and varies from 1.05 to 1.14 as velocity varies from 3 to 2.1 m/s.

The images taken so far do not show quantifiable deflection on jets passing through an NSTX-like outboard divertor for both 1D (toroidal) and 2D (surface normal) steady-state transverse gradient fields. This implies that the streamwise (axial) return current is not significant. The projected poloidal–vertical plan images of jet trajectories shown in Figs. 25 and 26 have been analyzed in detail to determine whether jets have deflected away from their axis. These images have been taken from the real images projected into a mirror placed at a 45° angle

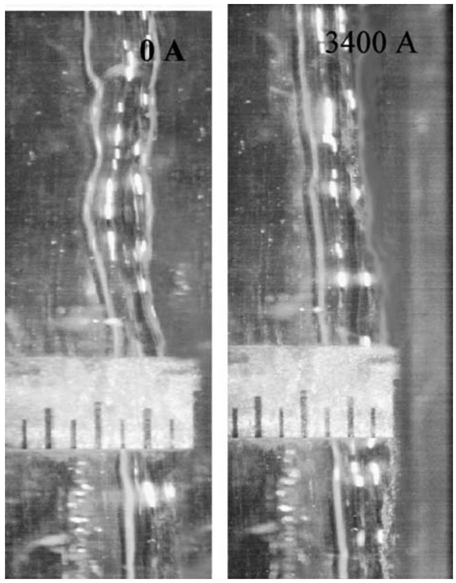


Fig. 25. Poloidal–vertical plan jet images with 1D magnetic field (jet velocity: 3 m/s).

on the side. These pictures indicate that the front edges of the jet maintain the same position even with the field turned on. This also shows that no jet deflection can be detected. These results reflect similar observations that

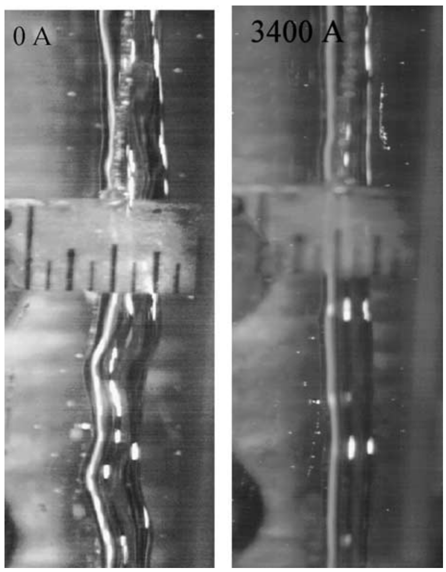


Fig. 26. Poloidal–vertical plan jet images with 2D magnetic field (jet velocity: 3 m/s).

have been numerically shown using FLOW-3D/MHD code (as in Case A analysis). Furthermore, the plot of the relationship between downstream location and positions of the jet edges indicates that with the magnetic field increasing, the oscillation in the jet edge location becomes less pronounced, while the mean position of jet edge remains the same.

Numerical calculations using the aforementioned FLOW-3D/MHD were performed to simulate experimental runs that were conducted at the UCLA MTOR facility. The computational domain includes a nozzle opening of 5 mm located at the beginning of the *x*-axis. The boundary conditions of the flow field are set continuous (except at the inlet boundary). All physical properties are those of GaInSn. Simulations were performed for inlet velocities of 3 and 5 m/s with MTOR 1D magnetic field configurations. The numerical results show similar MHD behavior as compared to experimental observations, including increases in jet radius and no observable deflection. However, the results slightly underestimate MHD effects and lead to a smaller reduction in jet radius (5.1% as compared 9% for the case of initial velocity of 5 m/s). Note that the width obtained from experimental measurements only accounts for the cross-section variation at the poloidal–toroidal plan.

## 4. Film flow characteristics under complex gradient fields

Film flow is also a possible candidate geometry for free surface module divertor application, in which a working LM, such as lithium, flows over a conducting or insulating substrate. A preliminary series of experiments without flux concentrators were performed with a 20-cm-wide insulated channel in order to study effects like channel filling and obtain data for validation of quasi-two-dimensional models.

In this series of experiments, the fluid is restricted laterally (toroidally) by two sidewalls with rather limited separation extent in the higher field of the flux concentrators in order to provide data to support a “module” design concept. In a toroidally segmented flow, the MHD effect is expected to be stronger from the toroidal field, since aspect ratio of the channel is much closer to unity. To the contrary, it is expected that MHD drag from the gradient surface normal field can be very significant, enough to stop the flow in a complete axis-symmetric flow. Experiments on a complete coverage axis-symmetric flow require a much larger liquid metal inventory and will be considered in the next stage of the study. Open-channel film flow experiments in MTOR require quantitative measurements of the free surface height—resolved both spatially and temporally. Previously, effort has been spent on developing a diagnostic system utilizing ultrasound to non-invasively measure the free surface height simultaneously at multiple locations [14]. The test section can be equipped with up to seven transducers driven through a multiplexer by one pulser/receiver box. The reflected signals are digitized by a fast (100 MSample/s) data acquisition card and stored in a control computer for later analysis.

For completely insulated walls, all electric current is confined within the liquid flow itself. While MHD drag can be significantly reduced for insulated free surface film flows, an electrically insulated coating will not be available within the proposed experimental time frame (i.e. 2008). Thus, it is prudent to know whether it is possible to establish a proper lithium free surface flow in NSTX magnetic field configurations using conducting walls. Presently, MTOR experimental investigations on liquid metal MHD free surface ramp flows are conducted for both insulated and conducting walls. The goal is to determine whether segmented film flows can overcome the MHD drag caused by NSTX-like gradient magnetic fields while achieving satisfactory operating conditions for particle and surface heat removal.

From a design point of view, free surface lithium flow over a divertor plate can proceed either from outboard toward inboard or vice versa. However, the large velocity required for particle pumping (as well as surface heat removal) implies that lithium carries a tremendous amount of inertia. To direct this energetic fluid away from the vacuum vessel without causing significant splashing to the plasma core requires a much larger space to house flow-guiding structures, which is not available in the cramped space at the inboard edge of the outer NSTX divertor region. Thus, the design for the NSTX outboard divertor module may call for lithium to be injected from the smaller radius (private flux region) outward toward the outboard, as shown in Fig. 1. A flow issuing from a higher field to a lower field will experience similar drag forces as one flowing in from the opposite direction. This alleviates MTOR experimental requirements since the space near the inboard of MTOR is extremely scarce. In experimental runs involving film flow with insulated walls GaInSn flows from the outboard toward the inboard. The space is made available through a design improvement to accommodate flow issuing from the inboard for film flow experiments with conducting walls.

### 4.1. Film flow experimental setup and test parameters

Two film flow test sections were manufactured with one being made from an electrical insulator (acrylic) and the other from a conductor (thin sheet 304 stainless). Both test articles featured compression nozzles with a 2 mm final height, are 45 cm long, and can accommodate the placement (and bracing) of permanent magnets and ultrasound transducers beneath the flow plan.

As shown in Fig. 27, the acrylic test article features a contracting flow area starting with an inlet flow width of 7 cm and tapered down to about 5 at 45 cm downstream. This is meant to address flow contraction issues that might be present in the strongly converging geometry of the spherical torus. The drain region in this test article proved to be limited to an inlet velocity of 1.1 m/s before the incoming fluid led to an overflow situation. One important requirement for establishing a viable film flow relates to fluid wetting capability; the fluid must be able to wet the solid substrate in order to achieve complete flow coverage [15]. Within the limited data available, the substrate was made from an acrylic sheet plated with a 0.1-μm-thick Inconel layer, its function being primarily to enhance wetting.

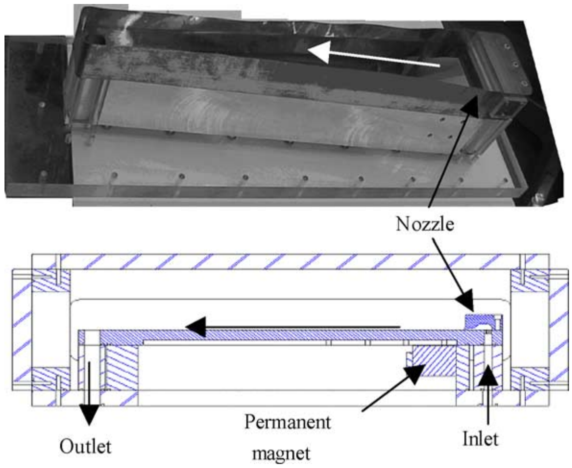


Fig. 27. MTOR film flow test section with acrylic insulated walls (top: actual test article; bottom: schematic view).

The electrically conducting test section, as shown in Fig. 28, is a constant 5-cm-wide and 45-cm-long channel constructed from a thin stainless steel sheet (0.5 mm thick). The inlet manifold includes a perforated plate to help distribute GaInSn flow more uniformly over the test area and a nozzle with a contraction ratio of five (defined as the ratio of inlet to outlet nozzle area) to

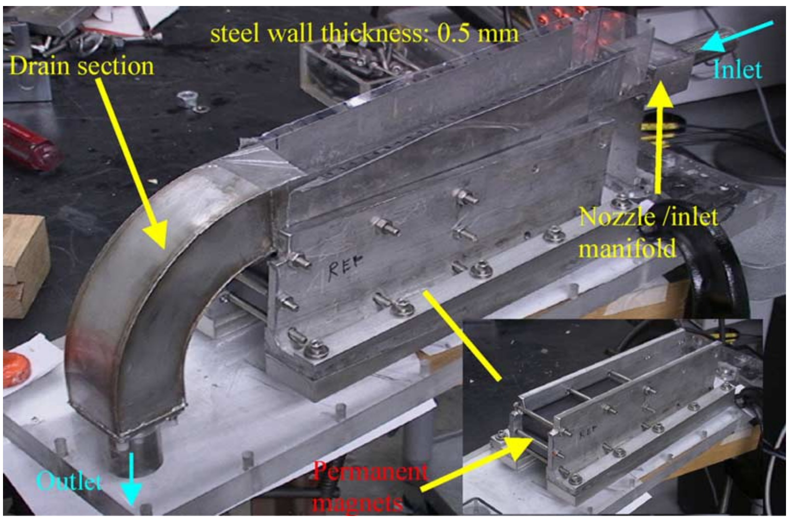


Fig. 28. Stainless steel conducting ramp test article (conductance ratio = 0.0067).

give a 2-mm-high flow at the nozzle outlet. In addition, to prevent GaInSn overshoot and to gradually guide the fluid toward the drain channel located parallel to the gravity direction, the test article substrate is curved 45° away from the flow plane near the outlet. A cover plate is welded to the test article drain section to catch any GaInSn overshoot. The conducting-walls test article has an adequate drain capacity to run experiments with inlet velocities up to 4.4 m/s.

To achieve a similar Reynolds number to that of lithium flow at 10 m/s, the nozzle outlet velocity must be 3 m/s for GaInSn. The flow rate will be varied around this value to explore a wider range of the *Re* parameters. In addition, these first experiments are being conducted to evaluate the possibility of flowing lithium "uphill" from the inboard higher field region to the outboard lower field region. The NSTX design concept allows lithium to be gradually extracted away from the chamber through a roomy outboard area without causing too much splashing and interference with CHI operation. The concept also implies that in NSTX's geometric configuration, lithium flows uphill ~17 cm over a 46-cm-flow path with an inclination angle of 21.5°. Since GaInSn is much heavier than lithium, the MTOR experimental setup forces GaInSn to climb uphill only about 2 cm to preserve the Froude number at the operating velocity of 3 m/s. As shown in Fig. 29, the MTOR experimental setup is near horizontal with an upward slight inclination angle of 1.85°.

The specific iron flux concentrators set used here creates a toroidal magnetic field varying from 1.2 T at the inlet to 0.48 T at the outlet. A surface normal magnetic field to the liquid flow is established downstream near the outboard end, by two permanent magnets, giving an average surface normal field of 0.3 T over a 12-cm flow-path. The magnetic field orientation and associated relative strength as seen by GaInSn as it proceeds from inboard toward outboard is illustrated in Fig. 30. The comparison of the scaling-corrected MTOR magnetic fields with corresponding NSTX field strengths (as in Fig. 31) indicates that the present MTOR field configuration is adequate to reveal any unfavorable MHD drag, if any exists.

### 4.2. Film flow experimental results

#### 4.2.1. Free surface ramp flow with insulated walls

Photographic images taken from the fast camera for LM MHD film flow characteristics with insulated walls show clearly how the magnetic field modifies film

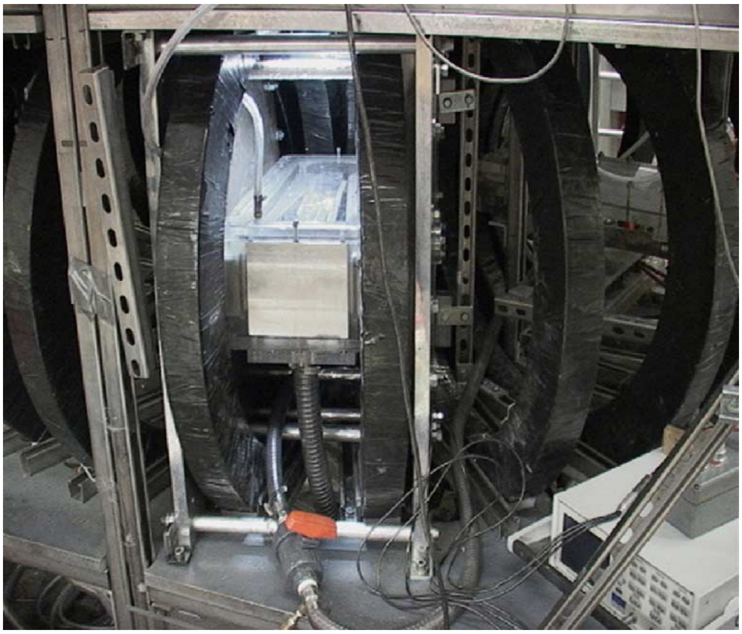

Fig. 29. MTOR experimental setup for proposed NSTX film flow concept evaluation.

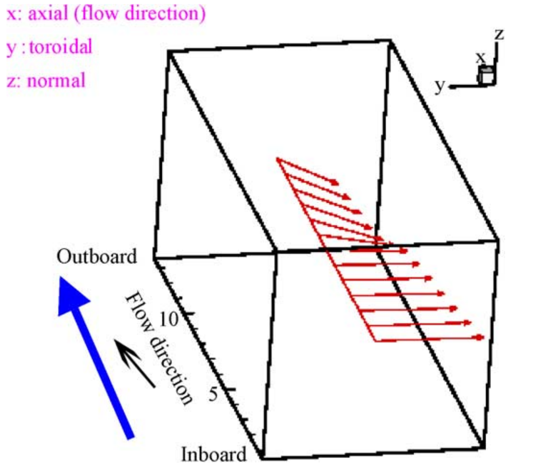


Fig. 30. Schematic view of MTOR 2D field orientation and relative field strength as seen by GaInSn.

flow surface structures. Here, GaInSn flows uphill at 1.85° away from the horizontal plan and issues from the outboard with field strength of 0.48 T to the inboard of 1.2 T at 45 cm downstream. The fast camera image of GaInSn film flow with a velocity of 1.1 m/s without magnetic field is shown in Fig. 32. As shown, GaInSn does not wet Inconel well and shows a tendency to pinch into the center of the channel, which results in bare zones near the sidewalls. With the magnetic field turned on, the deficiency of wetting has been completely erased while the fluid has been pushed to the sides and completely covers the channel. In addition, the effect of the magnetic field has significantly suppressed small-scale fluctuations and vorticity perpendicular to the field—resulting in a stretched vortex along the field direction. In response, the free surface of the film shows 2D wave structures along the filed lines (Fig. 33). Complete coverage of the flow channel is also achieved when the surface normal field is applied (see Fig. 34). The induced MHD forces eliminate the

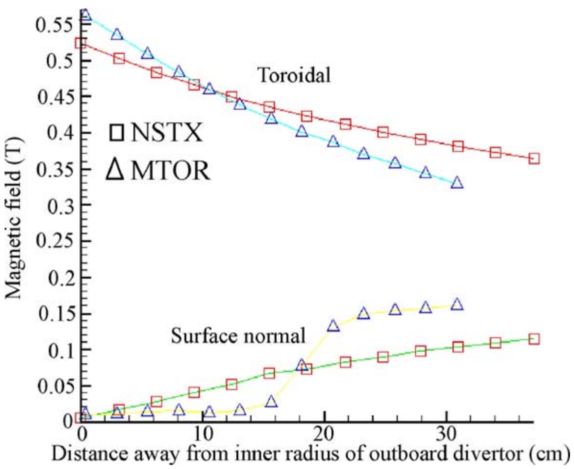


Fig. 31. Scaling corrected MTOR 2D fields, as compared to NSTX toroidal and surface normal fields.

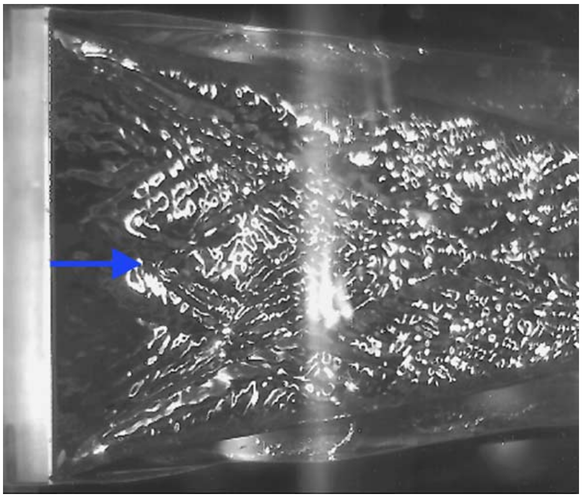

Fig. 32. Image of film flow free surface showing turbulent wavy structures (film initial velocity = 1.1 m/s).

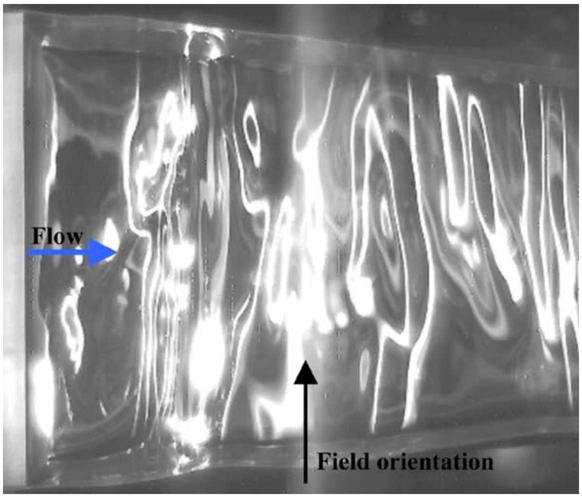


Fig. 33. Image of film flow free surface with 1D gradient toroidal field. Turbulent wavy structures seen in Fig. 28 have been suppressed significantly and result in 2D waves (film initial velocity = 1.1 m/s).

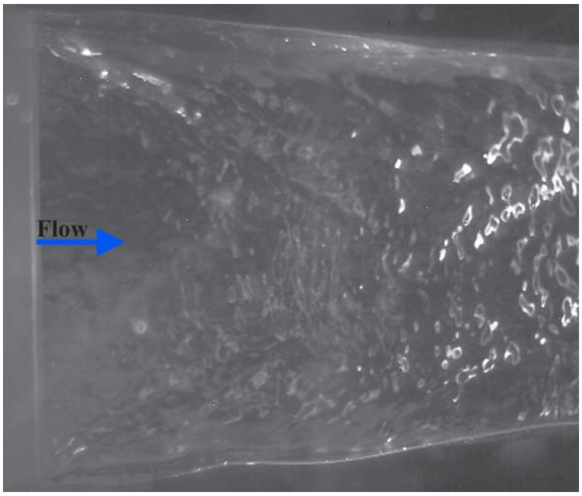


Fig. 34. Image of film flow free surface with surface normal field. Turbulent wavy structures near the inlet seen in Fig. 28 have been suppressed slightly by the surface normal field (film initial velocity = 1.1 m/s).

fluid's pinching and greatly modify the turbulent structures at the places where surface normal field is applied (the measured surface normal field is about −0.18 T at the substrate back wall). Only a limited number of runs were performed with this test section due to the limiting nature of the drain, but radical redistribution and bare spots due to MHD effects were not observed in this test section at the relatively low velocities explored.

#### *4.2.2. Film flow results of conducting walls*

Experimental results have been obtained for three different magnetic field configurations and are briefly described below.

1. A 1D toroidal field including field gradient. GaInSn flows uphill at 1.85° from the inlet with a field strength of 1.2 T to the outlet at 0.48 T at 45 cm downstream.

   The images in Fig. 35 from the high-speed camera looking directly downward at the flow going from left to right indicate that immediately near the nozzle outlet the turbulence is partially damped and markedly elongated 2D column-type surface structures are observed. However, as GaInSn alloy moves toward lower fields, these 2D rolling waves break down; while the fluid reverts back to its original 3D turbulent structures, as shown in the case of no magnetic field. At higher fluid velocity, 2D rolling waves persist to lower fields as shown in Fig. 36. In addition, it appears that the MHD drag caused by this magnitude of gradient toroidal field is not strong enough to significantly slow down the flow, other than modifying the flow structure as described above.
2. Same flow setup with a surface normal field only. Two permanent magnets are placed near the outlet of the test article to simulate the NSTX case where the surface normal field is the strongest. The setup gives an average surface normal field of about 0.3 T over a 12-cm-flow path starting at 18 cm away from the inlet.

   With a surface normal filed of about 0.3 T in the present experimental setup, the MHD drag opposing force (proportional to $\sigma u B_{\perp}^{2}$) appears to be significant enough to slow down the flow and cause the fluid to pile up. In addition, the flow is characterized with thick, streaky columns parallel to the flow direction. Film thickness traces from an inductive probe located at 28 cm downstream and 1 cm away from the sidewall indicate a factor of 2.25 increase in film height from the MHD drag produced by this magnitude of surface normal field. The trace in Fig. 37 shows a significant amount of fluctuation in film thickness at this specific operating condition. This fluctuation has been suppressed significantly when the fluid is subjected to additional gradient toroidal field when MTOR is operated at 2000 A (Fig. 37). By decreasing GaInSn velocity from 3 to 2 m/s the result is a further increase in film thickness by a factor 2.5. Clearly, decreasing velocity increases the interaction number, indicating that the magnetic forces dominate the inertial forces.

   A comparison illustrating the effect of magnet field orientation on LM MHD free surface characteristics is shown in Fig. 35.
3. A combined toroidal field from (1) with the surface normal field from (2).

   The image shown in Fig. 38 reflects a combined-added effect resulting from the gradient toroidal field plus the surface normal field. Near the outlet of the nozzle where only the toroidal field exists 2D rolling waves dominate the flow; however, as GaInSn alloy encounters a strong surface normal field, the fluid piles up and slows down as if it were frozen. Additionally, the flow appears non-

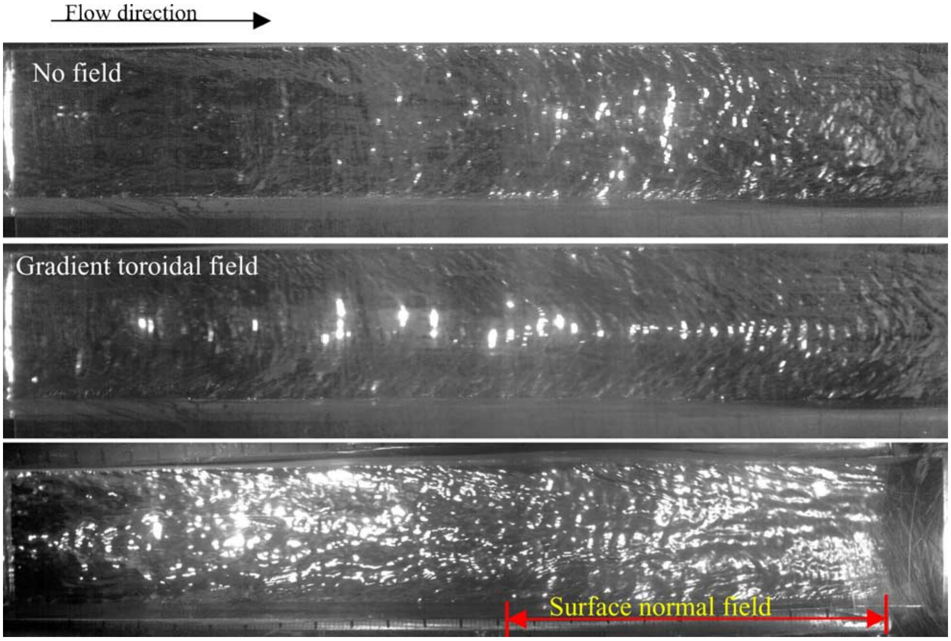


Fig. 35. Film surface patterns under different magnetic field conditions.

symmetric at 30 cm downstream where the surface normal field is significant, which may result from lateral forces caused by the induced axial return current interacting with the surface normal field.

With an inlet velocity of 2 m/s, quantitative measurements were obtained for film heights at six locations using the ultrasonic flow height measurement system. The MHD drag caused by the induced toroidal

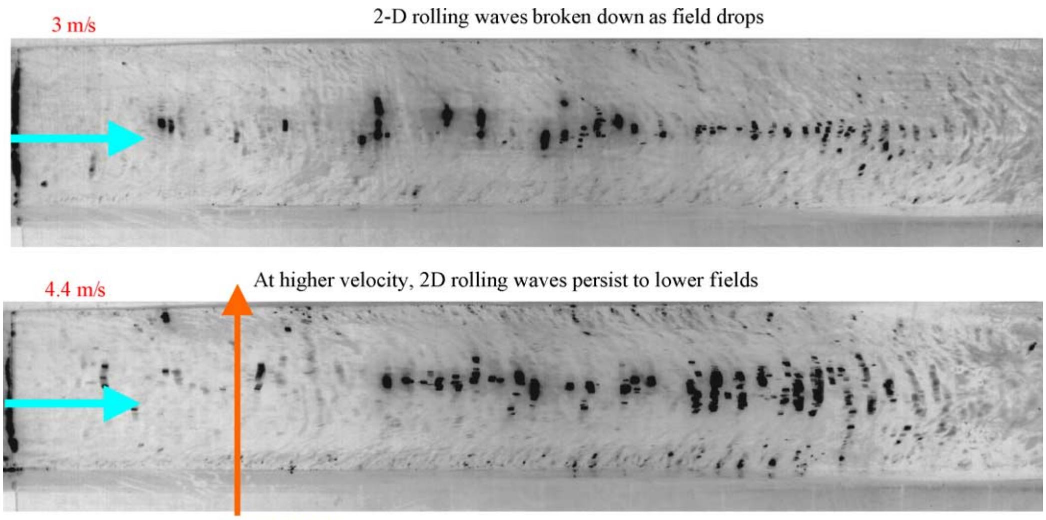


Fig. 36. Inverted images of wavy surface structures under gradient transverse fields for different initial velocities.

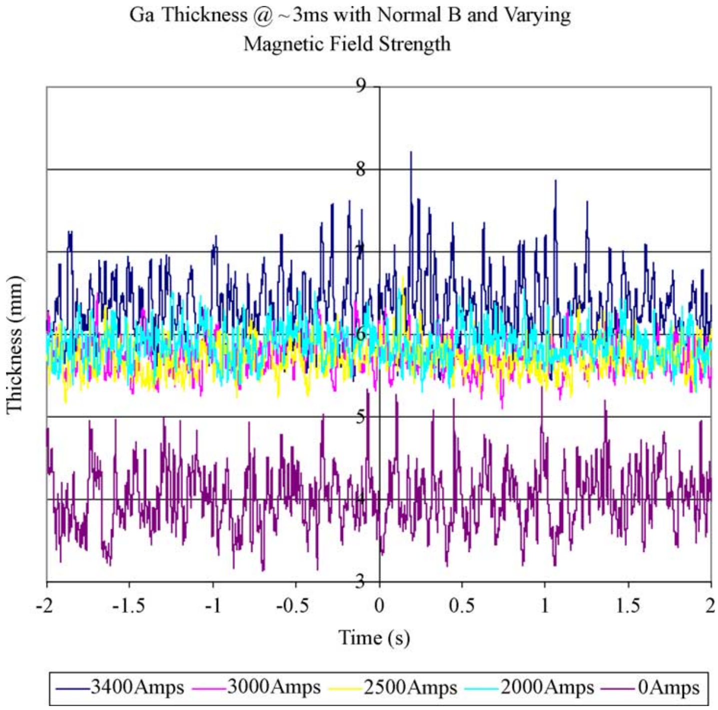


Fig. 37. Inductive probe signals of film heights at 28 cm downstream versus time for different coil current/magnetic field conditions.

current interacting with the surface normal field has resulted in an increase in film height by a factor of 3–4 times at 30 cm downstream, with the existence of surface normal fields only. The flow thickening is not uniform over the film cross-section as shown, so that one side of the fluid is about 40% thicker than the other side. Note that if the fabricated sidewall of the test article is leveled at the initial film height, then the presently observed increase in film height implies that the fluid spills over the sides of the module. This observation appears qualitatively consistent with the previous FLOW-3D/MHD calculations, where the results show that fluid spills over the side of the chute. An improved understanding is needed of the implications of non-uniform flow thickening and magnetic field-influenced surface turbulence structures on the use of liquid metal surfaces as divertor.

The ultrasound transducer fails to detect the reflective sound wave at a velocity of 2.5 m/s or higher, as the fluid becomes relatively turbulent. Turbulent fluctuation of liquid surfaces causes energy to be lost before the wave reflects back to the sensor (loss of signal). Presently, the film heights at high velocities are measured by the inductive probe, in which the film

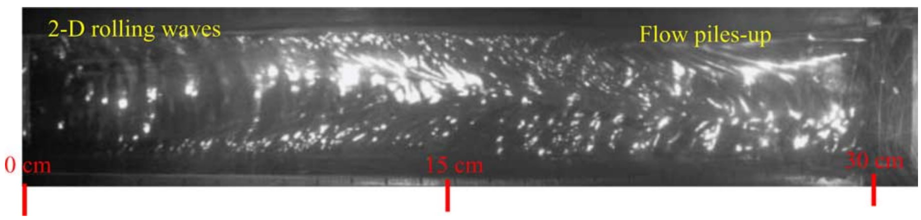


Fig. 38. Distinct wavy flow pattern appears as magnet field configuration becomes complicated (inlet velocity 3 m/s) (Field configuration values shown in Fig. 34).

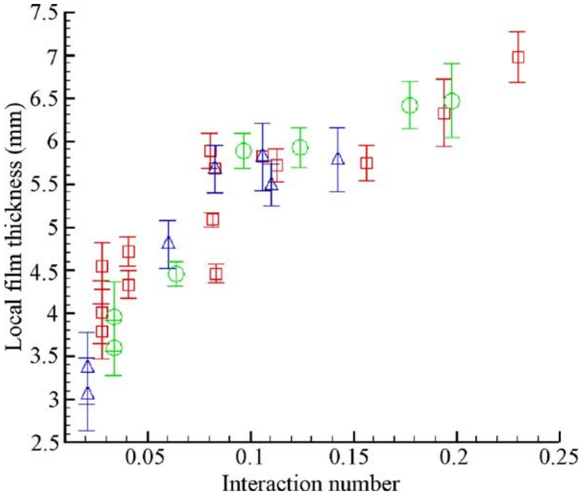


Fig. 39. Local film height as a function of interaction number at different film initial velocities (square: 3 m/s, triangle: 4 m/s, and circle: 2.5 m/s).

height change by the MHD drag is reflected through the change in the inductance between the film surface and the probe's face. The film height at 28 cm downstream and 1 cm away from one side of the wall with respect to different interaction numbers is plotted in Fig. 39. The interaction number is defined as

$$N = \frac{\sigma B_{\text{local}}^2 \delta_0}{\rho u_0}$$

where $u_0$ and $\delta_0$ are the initial film velocity and initial film height, respectively. Also, the $B_{\text{local}}$ is defined as: $B_{\text{local}} = \sqrt{B_{\text{T}}^2 + B_{\perp}^2}$. These initial data suggest that the local film thickness increase semi-parabolically (within the range of the experiments) with the interaction number and are not differentiable from the initial velocities. Since the field orientation has a distinct impact on the types of vorticity modification, the MHD effect may not be added linearly. Effort is underway to distinguish between the increase in the MHD induced film thickness by the spanwise field component from that by the surface normal component.

## 5. Summary and future plan

The proposed use of flowing liquid surfaces for divertor applications in the NSTX machine seems a very attractive option. Several key issues have to be resolved before the possibility of a module can be definitively established. A major issue is the MHD effect on the liquid metal free surface due to the existence of strong magnetic fields. This paper describes experimental investigations conducted on MHD liquid metal jet and film flows under NSTX divertor-like conditions at the MTOR facility at UCLA. The experiments are directed towards providing hard data for the APEX study to help evaluate the feasibility of a fast free lithium surface for particle and heat removal in a near-term physics device (e.g. NSTX). A gallium alloy (GaInSn) has been used instead of the actual working fluid (lithium) as the experimentation fluid due to safety considerations and ease of operation at room temperature. The flow inlet conditions, the magnetic fields and the flow dimensions have been appropriately scaled in order to obtain the same Reynolds Number (*Re*), Hartmann Number (*Ha*) and Froude Number (*Fr*) as proposed for a NSTX divertor module with lithium.

Experimental findings from the MTOR jet study indicate that the steady-state transverse field gradients have stabilized the jet, reduced turbulent disturbance, and delayed jet breakup. The MTOR NSTX-like magnetic field strength significantly stabilized the jet by suppressing velocity perturbations. Lorentz forces significantly modify vortex structure and reduce its intensity. Through this process the magnetic field stabilizes the liquid metal free jet and results in a delay of jet breakup. The induced axial current in the existing setup is symmetric, and no significant parallel magnetic field exists, which results in insignificant jet deflection. Note that these results are for GaInSn liquid metal jets issuing from an electrically insulated nozzle.

Important insights into the MHD behavior of liquid metal films under NSTX-like environments are also presented. It is seen that it is possible to establish an uphill liquid metal film flow on a conducting substrate, although the MHD drag experienced by the flow could be strong and cause the flow to pile up under simulated NSTX magnetic field conditions. The high inlet flow velocity required to establish the flow against the magnetic drag forces renders the flow turbulent. The magnetic field predominantly changes the turbulent flow structure that ranges from 2D column-type turbulence structures at regions of high magnetic field at the inboard to 3D ordinary hydrodynamic turbulence structures at regions of low field strength at the outboard. Another distinct phenomenon observed is the non-uniform thickening of the liquid film over the film cross-section. At present, the MHD drag in this 5-cm (narrow) chute causes a three times deceleration (or greater than three times increase in film height) on flow near the walls and partial stagnation towards the outboard end. Further understanding into the implications of non-uniform flow thickening and magnetic field influenced surface turbulence structures, and on the use and design of liquid metal modules as divertors, is needed. In addition, present NSTX plans call for a decision on the deployment of an LSM in 2006. With this extended time scale, it is possible to consider a fully toroidal LSM. This could avoid some of the boundary problems associated with modules of limited toroidal extent that were identified so far.

Future (near-term) experimental investigations will continue to focus on LM MHD film flow with conducting walls in a magnetic field region resembling a NSTX field configuration as seen by an outboard divertor lithium film. At present, the MTOR conducting wall test article size is limited by the magnet gap required for producing scaled field strength. The current test article width of 5 cm wide is much narrower than the size of any practical liquid-surface divertor module (e.g., 40 cm wide). A small-size test article implies a large conductance ratio, and thus a strong MHD boundary layer effect from the gradient toroidal field (although it has been argued that the corresponding MHD drag from the surface normal field would be less). Preliminary data from this small test module shows up to a factor of 3 increase in film height as the result of MHD forces. Such a fluid pile-up may not be favored since it would act as a “leading-edge”, which would be vulnerable to surface heating and result in excessive vaporization and possibly plasma disruption. A near-term goal would be to extend the module’s toroidal width via a power upgrade and operate the MTOR coils at their maximum current rating. This automatically produces a factor of 2 increase in MTOR field strength without the use of iron flux concentrators. Another option is to replace the GaInSn with lithium or a better lithium simulant, such as NaK. MTOR at its present power supply provides adequate toroidal width for larger module experiments or even for study with a complete toroidal coverage. Experiments for larger toroidal span test modules should incorporate downstream flow area expansion into design considerations.

In addition, the present set-up does not include the axial magnetic field, in which the induced toroidal current from the surface normal field can interact with this field component and produce a pulling force normal to a liquid surface. To ensure a complete assessment it may require adding an axial field component into to existing 2D-field set-up.

The effect of a time-varying magnetic field on MHD film behavior needs to be quantified, particularly the effects of prototypical field ramp-up and -down on MHD film flow behavior. The ramp-up time for the NSTX magnet is about 0.6 s. This is required to increase TF current through the 36 TF turns to its 71.2 kA maximum design value, which provides the full 0.6 T toroidal field at major radius $R$ = 0.854 m. Also, at the full current, the maximum “Equivalent Square Wave” time is only 1.3 s. After 1.3 s, it is necessary to shut down the coils to prevent overheating. It is known that the time-varying magnetic field can lead to a large emf and cause undesirable fluid acceleration (preliminary experiments with liquid jets showed that rapid power supply shutdown led to jet motion and breakage into droplets). To minimize emfs it may need to optimize the MTOR film test article layout (and thus provide useful data to NSTX LSM design). These aforementioned near-term experiments are essential to allow for the project to proceed with sound conceptual and engineering designs suitable for divertor particle pumping and surface heat removal applications in a near-term experimental plasma device, such as NSTX.

## References

[1] H. Kugel, et al., Development of lithium deposition techniques for TFTR, in: Proceedings of the 17th IEEE/NPSS Symposium on Fusion Engineering, 6–10 October, San Diego, CA, 1997.
[2] R. Manigi, H. Kugel, C. Skinner, Physics benefits of liquid metal usage and a review of tokamak experience with lithium, in: Presented at Workshop on Liquid Metals in NSTX, August 12, Princeton, New Jersey, 2000.
[3] M. Kotschenreuther, Recent Plasma MHD Results, Presented at APEX-11 Project Meeting at ANL, May 10-12, 2000.
[4] M. Ulrickson, et al., Liquid Lithium Surfaces for Particle Control, Presented at the NSTX 5 Year Plan Review, Princeton, New Jersey, 2002.
[5] N. Morley, S. Smolentsev, R. Munipalli, M. Ni, D. Gao, A. Ying, M. Abdou, Numerical simulation of liquid metal free surface MHD flow in the APEX study, this issue, 2003.
[6] Data calculated from EQDISK file for NSTX, PPPL.

[7] A. Ying, M. Abdou, S. Smolentsev, H. Huang, B. Kaita, R. Maingi, N. Morley, B. Nelson, M. Ulrickson, B. Woolley, MHD and heat transfer issues and characteristics for Li free surface flows under NSTX conditions, in: Proceedings of the 14th ANS Topical Meeting on the Technology of Fusion Energy [TOFE], Park City, UT, October 2000.

[8] M. Kotschenreuther, The effects of surface normal magnetic fields on concepts for fast surface flows of liquid metals, including toroidal breaks. APEX Memorandum, March 16, 2001.

[9] FLOW-3D User's Manual, Version 7.7, Flow Science Inc., 2000.

[10] H.L. Huang, A. Ying, M.A. Abdou, 3D MHD free surface fluid flow simulation based on magnetic-field induction equations, Fusion Eng. Des. 63–64 (2002) 361–368.

[11] X. Luo, A. Ying, M. Abdou, Experimental and computational simulation of free jet characteristic under transverse field gradients, The 15th Anmerical Nuclear Society Meeting, Washington, DC, 2002.

[12] N.B. Salah, A. Soulaimani, W.G. Habashi, A finite element method for magnetohydrodynamics, Comput. Methods Appl. Mech. Eng. 190 (2001) 5867–5892.

[13] P.A. Davidson, Magnetic damping of jets and vortices, J. Fluid Mech. 229 (1995) 153.

[14] J. Burris, Utilization of Ultrasonic Technique for Dynamic Measurements of Free Surface Flow Depths, UCLA, Master Thesis, 2002.

[15] N.B. Morley, J. Burris, The MTOR LM-MHD flow facility, and preliminary experimental investigation of thin layer, liquid metal flow in a 1/R toroidal magnetic field, Fusion Technol. 44 (2003) 74–78.

[16] R.E. Phinney, The breakup of a turbulent liquid jet in a gaseous atmosphere, J. Fluid Mech. 60 (1973) 689–701.

[17] I. Bucenieks, O. Lielausis, E. Platacis, A. Shishko, An experimental study of liquid metal film and jet flows in a strong magnetic field, Magnetohydrodynamics 30 (2) (1994) 179–187.

[18] S. Oshima, R. Yamane, The shape of liquid metal jets under a uniform transverse magnetic field, Magnetohydrodynamics 25 (1989) 273–279.

[19] V.M. Ievlev, A.S. Koroteev, V.B. Levin, The effect of a uniform magnetic field on stability, transition and turbulence as a control means for liquid metal flow mixing, Magnetohydrodynamics (1989) 161–166.

[20] J. Etay, A.J. Mestel, H.K. Moffatt, Deflection of a stream of liquid metal by means of an alternating magnetic field, J. Fluid Mech. 194 (1988) 309–331.

[21] M.J. McCarthy, N.A. Molloy, Review of stability of liquid jets and the influence of nozzle design, Chem. Eng. J. 7 (1974) 1–20.